UNIVERSITY OF TWENTE.

Faculty of Engineering Technology
Department of Biomechanical Engineering

Modelling of Robotic Hands: Kinematic and Dynamic Parameter Identification

Víctor Antonio Carmona Ortiz

M.Sc. Thesis

Document Number: BE - 906
23rd November 2022

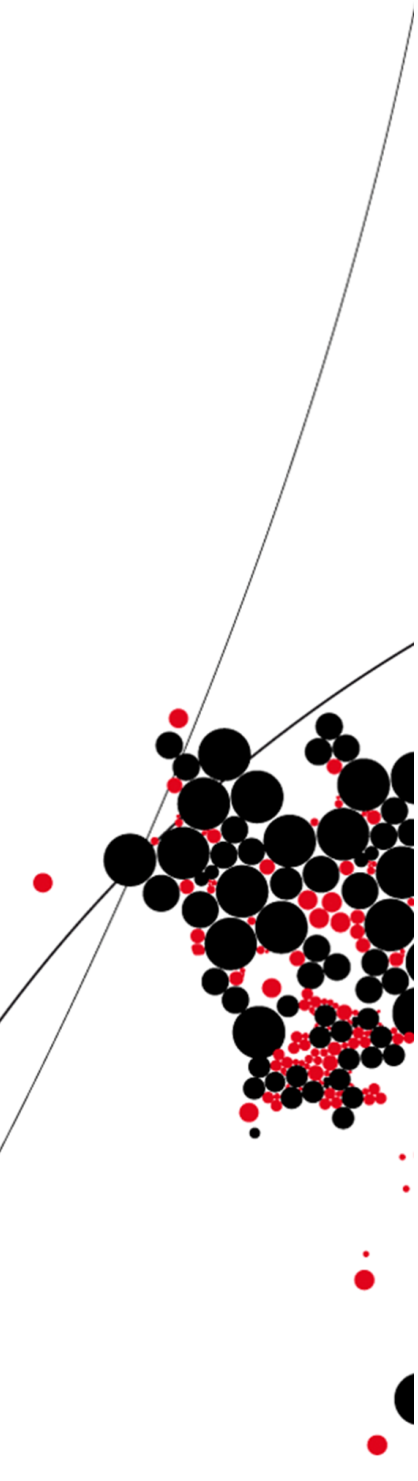

Supervisors:
prof. dr. ir. M. Vlutters
ir. A.H.G. Overbeek
Commitee:
prof. dr. ir. H. van der Kooij
dr.ir. W. Roozing

Biomechanical Engineering
Faculty of Engineering Technology
University of Twente
P.O. Box 217
7500 AE Enschede
The Netherlands

Acknowledgments

I would like to thank my supervisors prof. dr. ir. M. Vlutters and ir. A.H.G. Overbeek for their dedication, guidance and support during the development of my thesis. I would also like to thank all the members of the Nakanama Lab that have been part of this journey, to them, my best wishes. Finally I would like to thank my friends, housemates and family for their constant love, support and energy.

Abstract

One of the features that characterizes human versatility is the capability of object complex manipulation. Humans owe part of this capability to the mechanical design and sensory system of our hands. With the advanced performance of human hands on manipulation tasks, researchers have started to develop manipulators that mimic human hands. In order to develop controllers for such manipulators and integrate them into robotic devices it is useful to develop models of the system. This work presents the development of a kinematic and dynamic model of robotic hands. In an experimental setup, a motion capture system is used to obtain finger motions of a pair of prosthetic hands. From the motion capture data and data from the hand sensors, an estimate of the centers and axes of rotation of the finger joints that represent the kinematics of the hands. Furthermore, a dynamic model is derived from data related to the current and the motion of the actuators in the hands. The validity of the models is assessed showing the advantages and future lines of research that this model opens.

Contents

List of Figures

List of Tables

Chapter 1

Introduction

One of the main challenges in robotics is the interaction with the environment in a safe and secure way. The world has been designed by humans, for humans. From simple stairs, to furniture or tools, everything has been designed for the practical use by humans. Robotic devices, regardless of their design, must be instructed to adapt to our world in order to be able to optimally perform substantial tasks [2]. Up until now, task-specific designs for robots have proven to be an effective approach in industrial controlled environments. However, the aim for the introduction of robots in human-robot collaborative environments has generated a demand for robots with a general-purpose design.

In this context, humanoid robots show a greater potential versatility when compared to quadruped, wheeled or flying robots. While these last examples can outperform humanoid robots in certain environments, human-like designed robots can conceivably adapt to a greater range of purposes [3]. One of the evolutive traits that made humans so versatile is the anatomy of our hands. Allowing for complex manipulation of objects, our hands broaden the number of ways in which we interact with our surroundings. The combination of several degrees of freedom both within the fingers and the palm of the hand, and the ability to actuate most of them independently, provides humans with the capability of easily manipulating objects of different shapes and sizes.

In addition to the mechanical morphology of the human hands, the sensory system of the human body increases the manipulation capability of objects with different compliant behaviours. One of the most important features of human hands, and in great part, responsible for their versatility, is the ability to feel physical properties of objects such as their shape or the material they are made of. With the advanced performance of human hands on manipulation tasks, researchers have started to develop manipulators that mimic human hands both in mechanical and sensory design, which yet again, can conceivably adapt better to a human designed world [4]. All these developments aim then, to improve robot dexterity in manipulation tasks.

The main difference between general manipulators and dexterous manipulators is that dexterous manipulators show object-centered behaviour, which can only be accomplished with precise motion-and force control [5]. As stated in [6], two main control strategies allow for an implementation of human-like contact for manipulation: *hybird positon/force control* and *impedance control*. Both methods control directly or indirectly the force applied by the end effector of the robot, in this case the fingers.

In order to accurately implement these control strategies on real robotic hardware, it is useful

to have information on the physical properties of the system, i.e. a system model. In the first place the model of the system establishes constraints on the type of contact between the manipulator and the object, which will in turn change the application of the force on the object. Moreover, a system's model is often a simplified version of the real physical system, which allows for testing of the designed controllers in simulation environments, reducing risks of damaging hardware or costs during testing phases. For commercialised products, these models might not be provided/available.

This work presents the identification of kinematic and dynamic parameters of a commercialised prosthetic hand, the BeBionic hands [1] in order to develop a model that can be implemented in robotics systems. The models contain a full description of the joint origins and joint axes of rotation describing the kinematics, and an approximation of a dynamic model based on unit-less signals provided by the hardware. Both models represent the first steps towards the integration of advanced hardware in order to extend the off-the-shelf capabilities of a humanoid robot aimed to be deployed in human-collaborative environments.

1.1 Framework and Motivation

The presented work is the application of parameter identification techiques in robotic systems. The modeling of the kinematics of this prosthetic device will allow for an improvement on the functioning of an off-the-shelf robotic system. This work will be used to improve the task span of a commercialised humanoid robot, making the robot more dexterous and useful inside any environment. The Nakama lab is trying to implement machine learning and robot-human interaction strategies to be able to adapt the humanoid robot EVE [7] with the aim of introducing the robot in healthcare environments. In order to do this, EVE must be able to interact safely both with the physical environment in hospitals and nursing homes.

The inclusion of robotic hands as manipulators for EVE, will provide the robot with the ability of fine manipulation of objects. In addition, the ability to sense external objects physical properties will further extend the EVE's manipulation abilities allowing for the interaction with fragile equipment. The first step towards the insertion of this model in EVE's framework is the development of kinematic and dynamic models such that the robot can communicate and control the configuration and dynamic behaviour of the hands. Furthermore, the inclusion of such model will open a possibility to include the hands in simulation environments in combination with models of EVE. This establishes a starting point for the application of control strategies in EVE for object manipulation and interaction before applying these in a real setup with the actual hardware.

1.2 Research Questions

- Can we use motion capture data to derive a kinematic model of the BeBionic robotic hands?
- Is it possible to compute a unitless dynamic model that can predict a force-related signal on the BeBionic hands, such that it is possible to distinguish the presence of objects interacting with the hands during grasping tasks?

1.3 Report organization

The following report describes the data gathering and processing for the development of a digital kinematic of a pair of prosthetic hands to be coupled with a humanoid robot. Chapter 2 provides the necessary background in the form of a literature study for the reader to follow the methodology implemented. Chapter 3 describes the methods utilised for the collection of kinematic and dynamic data as well as the processing of this data into a sensible useful model. At the same time, this chapter displays the reasoning for the decisions made during the model development. Chapter 4 describes a qualitative and quantitative analysis on the parameters obtained. Lastly, Chapter 5 discusses the validity of these findings as well as the the flaws and major improvements to be implemented in future extensions of this work.

Chapter 2

Background

2.1 Literature Review

This section provides an overview of the knowledge needed to follow the methodology implemented during the development of the thesis. The development of kinematic and dynamic models for robotic systems is introduced, together with a review of the relevant literature related to these topics. The literature regarding modeling based purely on design parameters is left out as it might not be relevant for this work. A review on identification of the kinematic and dynamic parameters of biological/robot systems is presented, showing the similarities between both fields of study.

2.1.1 Kinematic Modeling and Kinematic Parameters Identification

The description of robot kinematics is a well established problem. The kinematic modeling of robotics systems provides a representation of the motion of bodies in robotic systems disregarding the forces or toques that cause this motions [8]. Since the appearance of the first robotics systems, the field of robot kinematics has been extensively studied, giving birth to several standardized methods such as the Denavit–Hartenberg parameter convention, or the more modern screw theory based methods. Each of these definitions show advantages and disadvantages compared with each other [9].

The main goal of the study of robot kinematics is to find the relation between the joint Space (joint angles and angular velocities) of a robot, and the Cartesian space (end effector's position and velocity). This relation can be expressed in the form of *forward kinematics* (FK), where given the configuration of the robotic joints the corresponding end effector configuration is computed. On the other hand, the study of *inverse kinematics* (IK) finds a set of possible joint configurations given a certain end effector state.

This mapping between Joint space and Cartesian space is dependant on the physical properties of the robot. Joint origins, segment lengths and actuation axes allow for the complete definition of the kinematics of robotic systems. While the robot designers generally provide a model for the robot, these models might lack accuracy due to manufacturing problems or inaccuracies. Thus it is necessary to perform a calibration procedure to find that these parameters are correct.

The approach to this problem has been tackled similarly in biomechanical modeling research,

where researchers model human musculoskeletal systems as a series of interconnected rigid bodes in the same way as a robotic system. Intuitively the same approaches can be translated from the field of biomechanics to the field of robotics as shown by [10]. In both fields, research looks for the same solution, finding the parameters that describe the kinematic chains of robots/human limbs, defined with the general terms: **Centre of Rotation (CoR)** and **Axis of Rotation (AoR)**. In literature, CoR refers to the origin of a combined joint spanning more than one DoF, as generally, rotary joints are described by their AoR. However, it is still necessary to find an approximation of the CoR for these type of joints in order to have al the information of the kinematic chain.

Regarding the identification of the CoR, Zang et al. [11] and Won and Lee [12] developed complex geometrical models for the identification of kinematic parameters of human hand fingers. Both studies utilise optical motion capture systems to obtain kinematic data of real human hands in order to assess the validity of their methods.

Ude et al. [13] utilize a screw theory approach on the modeling of human joints as hinge joints, since their main goal is to map human motion to robot motion based on rotary actuators. Their approach uses the product of exponentials to build a cost function used to minimise the computed position of certain markers in a global reference frame compared with this position measured by an optical motion capture system. One of the main disadvantages of this study is the lack of repeatability of the original pose needed to construct the kinematic chain.

O'Brien et al. [14] and Tuceryan et al. [15] show similar approaches using a classical kinematic description. In both studies, the fact that a joint location should be the same when observed from two different reference frames and transformed properly. The approach taken [14] relies on the observation of the CoR of a joint from its adjacent links, for which the point is static regardless of the relative motion between links. The approach taken by [15] physically fixes a point in space and uses that point as CoR, rotating the link of interest around that point and using the position of the point in local reference frame and in the global reference frame for their cost function. This approach is known as *hotspot calibration* as referred in [10].

Ultimately, Chang and Pollard [16] propose a non-rigid sphere fitting to a point cloud generated from a set of points assumed to be on the surface of a sphere. The solution turns out to be a constrained least squares (LS) problem. The authors show that this approach can be applied in biomechanical frameworks, based on multi-marker motion captures. This approach is ultimately chosen to be applied in this work, appendix A shows the derivation of the cost functions formulated in [16].

With regard to the identification of the AoR, two main studies were analysed. The first one produced by Gamage and Lasenby [17] propose a cost function based on the assumption that a set of points attached to a rigid body that rotates around a revolute joint describing concentric circles. The line passing through this centre is the AoR. This results in a linear equation, the solution of which can be found using techniques as SVD.

In a similar fashion, Chang and Pollard [18] improved the work carreid by Gamage and Lasenby defining a combination between a planar and a radial cost function, which improved the estimation of the AoR compared to the previous mentioined work, specially for motions in which the rotation around the AoR was mixed with a secondary rotation around another axis. While the improvement achieved in [18] is substantial under certain conditions, for the problem at hand this is not of high relevance, as the rotations are mechanically constrained by the physical design of the prosthetic hands. Taking this last point into account, and due to its simplicity and effectiveness, the approach developed by Gamage and Lasenby is im-

plemented during the present work. The derivation of the equations from [17] is shown in appendix A.

2.1.2 Dynamic Modeling and Dynamics Parameters Identification

The two main and most common approaches are based on Newtonian or Lagrangian mechanics. Robot dynamics is the study of the relation between the forces/torques acting on a robotic system and the motion caused by these. These are affected by both inherent physical properties of the robot as its mass, moments of inertia, or friction present on its actuators. In addition, these dynamics must take into account kinematic information, such as the configuration of the system at a given time instant, as the combination of these and its properties will have an effect on the forces acting on itself.

In a similar fashion as in the previous section, the relation between the forces and the motion of the robot can be expressed in the form of *forward dynamics* (FD). FD express the motion of a robotic system as a function of the forces applied on it. On the other hand, inverse dynamics (ID) are used to compute the required forces in the Joint or Cartesian space in order to produce a certain motion.

Regardless of the approach taken, the same equations govern the dynamics of robotics systems. A common equation when modeling robot dynamics is equation 2.1, from Lagrange equation. The terms $M(q)$, $C(q, \dot{q})$ and $G(q)$ represent the configuration-dependant inertia matrix of the robotic system, the Coriolis and centrifugal forces, and the gravitational forces acting on the robot respectively. In the same equation $q, \dot{q}$ and $\ddot{q}$ represent the joint positions and their derivatives, and τ the froces and torques acting on the system. This parametric description of a robotic system can represent its whole dynamic behaviour given the correct parameters.

$$M(q)\ddot{q} + C(q, \dot{q})\dot{q} + G(q) = \tau \tag{2.1}$$

The rather complex representation of equation 2.1 is suitable for the representation of a generalised dynamic model of a robotic system despite its highly nonlinear nature. Simple robotic systems with limited actuators and degrees of freedom might show dynamic equations with non-configuration dependant parameters. This is the case for simplistic mechanisms that can be represented in 1D, where the dynamics are represented by equation 2.2. Where I, b and τ_{ext} represent the inertia, friction coefficient and external forces acting on the system, non dependant on the configuration of the system.

$$I\ \ddot{q} + b\ \dot{q} + \tau_{ext} = \tau \tag{2.2}$$

This equation is linear on the parameters. The main problem with equation 2.2 is the assumption of linearity of the friction term, described by $b\ \dot{q}$, as even in the simple case of 1D dynamics, friction is highly non-linear. The nonlinear nature of friction forces has been a field of study on its own. Three models developed between the late 1700s and mid 1800 are still used to model friction in modern engineering [19].

As the physical parameters of the robotic system are relevant to the description of its dynamics as seen from the equations above, it is crucial to have an accurate value for these. Robotic systems designers do not always provide a physical model of the robot. Moreover, fabrication and assembly processes can make these vary. For this reason, researchers have

focused on the development of approaches to accurately obtain values that allow for a faultless description of the robot dynamics. In order to do so, most of the literature reviewed show similar approaches, showing the advantage of having linear/linearised models.

The approach chosen by several researchers is the utilisation of linear least squares minimisation. Antonelli et al. [20] describe a systematic approach to this problem where an example of the identification of a linear model of a rigid manipulator with successful results. Kawasaki and Nishimura [21], Chan and Chen [22], and Grotjahn et al. [23] although in slightly different ways, use this same approach, showing that this approach results effective in the identification of dynamic parameters.

2.2 Setup description

The Hands: Ottobock BeBionic

The BeBionic hand (fig. 2.1) is an anthropomorphic multi-articulated prosthetic device with myolectric control primarily ment to use as a prosthesis. The company provides a set of 2 or 4 surface electromyography (sEMG) electrodes as an interface with the prosthesis. The hand provides 14 different pattern grips with different modes of control, all of them based on proportional speed control for a fine natural control on precision tasks. As additional interfaces the BeBionic hand contains a button on the reverse of the hand that allows for its activation and deactivation when holding it pressed. The external button allows for grip pattern modification when the button is simply toggled. Moreover, the prosthesis allows for Bluetooth connection with smart devices in order to preform al the aforementioned tasks using their personalised interface.

Figure 2.1: BeBionic prosthetic hand commercialised by Ottobock [1]

Mechanical Design

The BeBionic has an antropomorphic design, imitating the shape and function of a real human hand. It has 5 actuated fingers distributed on the palm of the hand, and a total of 6 degrees of freedom (DoF). Each actuated finger is controlled by a motor embedded inside the palm of the BeBionic hand except for the thumb, which contains the motor inside the same finger structure. The actuation methodology of each finger is not completely known, however based on reasonable assumptions each of the motors is coupled to each finger through a high reduction gearbox. The reason for this assumption is the relatively high force-to-size ratio of the actuators, as the space available for them is limited. The actuators used in the BeBionic hand are linear, generating the motion as follows.

Each finger is divided into two segments, both coupled to the palm of the hand, and to each other. Defining the palm as a fixed element, the two segments of each finger are attached in series to the palm. In order to generate the rotary motion around the points of attachment between segments, the actuator is attached to the first segment such that the linear motion of the actuator produces a moment around the rotation point between the palm and the first segment. In a similar fashion, a rigid bar is attached between the palm and the second segment such that the restriction imposed by the bar induces a rotation of the second segment with the motion of the first segment. Figure 2.2a shows a diagram of the described mechanism. To finalise, it is important to mention that in order for the hand to be more robust against impacts, the mechanical design allows for free movement of the fingers of the BeBionic with respect to the actuator for flexion motions, as it can be seen in figure 2.2b. To ensure that the finger is constantly coupled to the actuator while no other force is acting on the fingers, the fingers are spring loaded. This creates a constant load against the motors during the closing of the hand, but an assistive load during the opening.

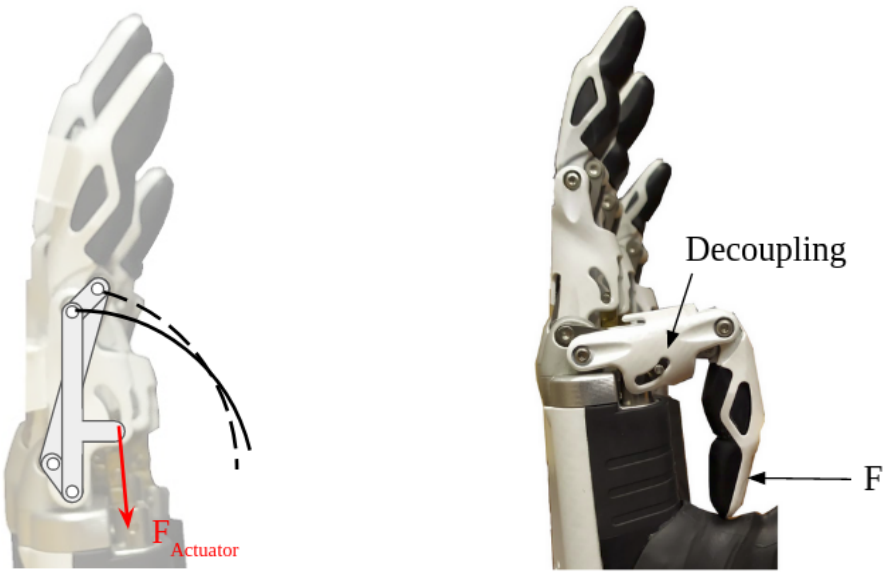

(a) (b)

Figure 2.2: (a) Mechanical design of the hands, the physical constraints of the linkages between the segments generate a relative motion between both finger segments. (b) Decoupling of the actuator from the finger when external forces are applied enforcing finger flexion.

Control

The BeBionic hand contains embedded low level controllers for position, velocity and force. However, there is no access to those controllers or the signals these are based on. A high level control interface has been provided by Halodi [7], who integrated the hands into the robot's control structure, together with Ottobock. Given a certain set point, desired speed and maximum current, any finger will follow those commands until reaching the set point. Information can be extracted from the hands related to the position of the motor and its current, nevertheless, none of these values hold physical meaning. The position values, as well as the set point to be sent must be provided as a floating point from 12000 to 18000 approximately depending on the finger. For the velocity values to be specified an integer from 0 to 255 must be provided, similarly for the current.

Chapter 3

Methods

This chapter describes the methodology followed to perform the identification of the kinematic and dynamic parameters of the BeBionic hand. The proposed methodology makes use of multi-camera optical tracking system to obtain information about the configuration of the BeBionic hand in 3D space. First section 3.1 describes a tool crafted during the research and its basic principle and purpose. This tool was used in several occasions through the experiments, providing relevant data to the development of the model. Next, in section 3.2 a description of the kinematic data collection is depicted with a description of the setup used during the motion capture. In addition, this section describes the approach taken for the identification of dynamic parameters of the BeBionic hand. The data acquisition procedure is thoroughly described followed by the data post processing approach in section 3.2.2.

Following, section 3.2.3 presents one of the main problems found during the data processing is described and the utilization of the previously described tool with the intention to solve it. Next, section 3.2.4 the reconstruction of the contact surfaces of the hand with the help of the same tool is depicted.

Moreover a description of the parameter fitting approach is given. Next, a description of the dynamic models to be fit to the gathered data is described in section 3.2.5. Finally, in section 3.2.6a set of validation steps is described to verify that the models obtained are competent. A set of error metrics are described to assess the validity of the kinematic model.

A similar process as the one described is followed for the identification of the dynamic model. Section 3.3 introduces the dynamic modeling identification procedure followed by the data pre-processing carried out. Next, 3.3.2 introduces the models chosen as candidates to represent the dynamics of the hands, followed by the explanation of the parameter estimation approach in section 3.3.3. Lastly, an experiment to evaluate if the dynamic model can detect objects when grasping is introduced in section 3.3.4

All the data processing was performed in python environment. A data object **.hand* was created containing all the information for each hand and segment, from motion data to kinematic parameters.

3.1 Probing Tool

Through the process of the data gathering and processing, several problems where encountered, for which it was decided to create a tool that allowed for precisely capture 3D points in space. These problems will be addressed in each section, as well as the utilisation of the tool to overcome them. The tool was modified by the Biomechanical Engineering department at the University of Twente. It consists on a *"T"* shaped structure with a total of 4 reflective markers attached to it distributed as shown in figure 3.1. The main principle of the tool is based on the reconstruction of rigid bodies obtained from multi-camera optical tracking systems data. First, a definition of the marker distribution on the probe is needed. In order to do so the following steps should be followed:

1. Stick *n* number of markers on the prove on a non co-linear, non-symmetric disposition
2. Select the point (here the tip) which will be reconstructed during the data collection process
3. Define the local positions of the rest *n-1* markers with respect to the reconstructed point

After the definition of the rigid body, the reconstruction process is performed applying the Kabsch algorithm [24], that minimizes the root mean squared deviation between two 3D point sets. The Kabsch algorithm provides information on the rotation and the translation from the original point set to the translated point set. The translation provided by the Kabsch algorithm is the reconstructed point for the rotated point set. In addition the tip of the tool (lowest part in figure 3.1) was filed into a conic shaped point to help at precisely point into structures of interest.

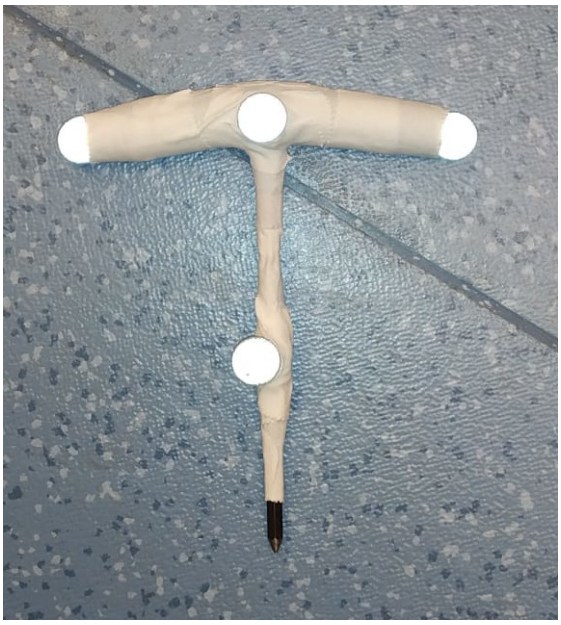

Figure 3.1: Proving tool utilised for the reconstruction of 3D points in space

3.2 Kinematic Model Identification

The relative rotation between the different segments of the BeBionic hand has to be computed, so that the *CoR* and *AoR* of a joint between two adjacent links can be computed. The methods utilised for the computation of the kinematic parameters rely on the assumption that the data points of interest perform a circular motion around a specific point in space. In the case of the BeBionic hand, five different kinematic chains can be described, one for each finger. Each of these kinematic chains contains 3 links connected in series: the palm of the prosthesis, and two consecutive phalanges, all connected through hinge joints. Motion captures of 40 seconds where performed with a total of 9 markers in frame (three on the palm and three on each finger), while each finger was commanded to generate flexion/extension motions consecutively with the full range of motion for each finger. In the special case for the thumb, where there are two possible configurations, and so 4 different AoRs and CoRs. The motions were performed in both configurations, adding to a total of 6 motion files.

Within all these files, the data was expressed in the global coordinate frame of the multi-camera optical tracking system. During the motion capture procedures, our interest relies on finding a constant point and axis around which each finger segment rotates, howeverbecause the hand might not be static w.r.t. the world referenc frame, mismatches between the values of interest might appear between frames. It is important then, to define a reference frame on each segment, such that the motions recorded are expressed with respect to a chosen reference frame, regardless of the changes in position and orientation of the hand. It is sensible then, to define a reference frame in the first segment of the kinematic chain attached to a CoR of interest. In the case of the first joint, the reference frame was defined at the palm. For the second, most distal joint, the reference frame was defined on the first finger segment.

3.2.1 Hand Frame Definition

Two different frames of reference were defined from the palm of each hand, a marker based frame and a landmark-based frame. Three markers where attached the the back of the palm of the hand so that a consistent reference frame could be defined over the frame set for each capture. The landmark-based frame was defined using the tool described in section 3.1. Three identifiable landmarks on the back of the palm of the hand were selected for the same reason as the marker-based frame. These landmarks consisted on either indentations or corners, figure 3.3 shows the selected landmarks.

Marker Based Frame Definition

Three relatively distal locations on the palm of the hand were chosen to stick the frame-definition markers, as the longer the distance between the markers the less sensitive the frame definition will be to noise on individual markers. Two markers were placed between the little-and the ring fingers, and the index-and middle fingers as shown in figure 3.2. These markers are referred to as *lateral* marker (p_l) and *medial* marker (p_m) respectively. The third marker was placed on a flat surface on the proximal part of the palm, near the wrist of the prosthesis. This marker is referred to as *origin* (p_o). This naming convention was followed for both hands, taking into account that the positions of the medial and lateral markers are swapped with respect to the origin marker for a pair of hands. The palm frame based on

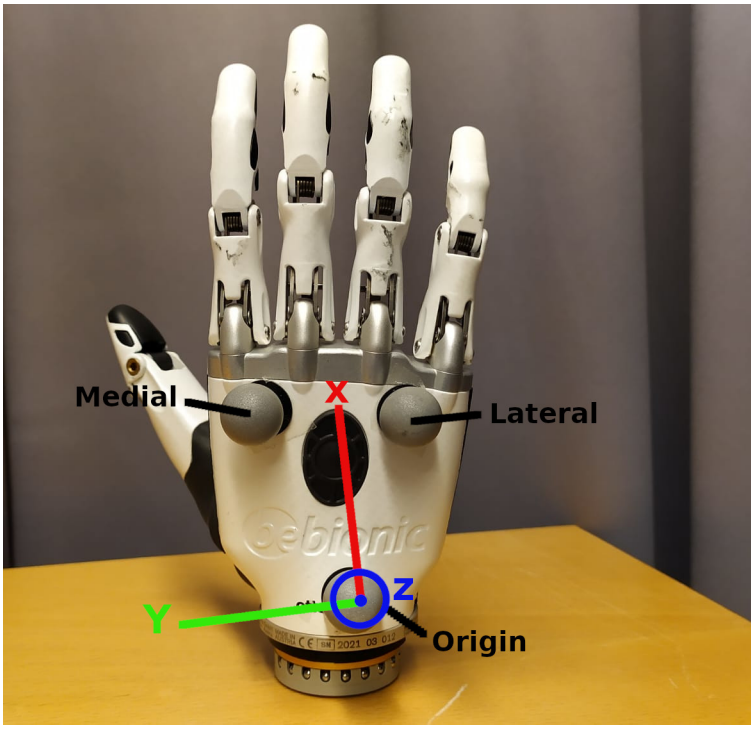

Figure 3.2: Position of the marker based frame. The naming convention per hand is modified in accordance to the mirroring relation between both hands. A representation of the defined axes is depicted.

these markers was defined as follows. The first vector v_z of the frame is computed from the cross product of the vectors from the origin to each of the distal markers:

$$v_z = (p_m - p_o) \times (p_l - p_o) \tag{3.1}$$

Again taking into account the mirrored relation between left and right hand, where the order of the cross product is swapped. The second vector v_y is defined from the cross product of the computed v_z and a vector defined by the mean position between p_m and p_l from the origin p_o:

$$v_y = v_z \times \left[\frac{(p_l + p_m)}{2} - p_o \right] \tag{3.2}$$

This ensures orthogonality between v_z and v_y. Lastly, the cross product between these two vectors defines the last vector of the frame v_x. Ensuring orthogonality between the three vectors.

As stated before, as set of rotation matrices and translations was defined per frame set, to transform all the data to this defined frame, with the origin marker position as the translation vector:

$$R^i = [v_x^i v_y^i v_z^i] \quad , \quad t^i = p_o^i \tag{3.3}$$

Provided that the vectors v_k^j are column vectors, where the superscript i in equation 3.3 states the frame of the capture being processed with respect to the reference frame in which the vectors are defined.

Repeatable Frame Definition

While the definition of a marker-based reference frame comes in handy when expressing relative motions between segments, it lacks a component of repeatability. In the case that these captures where performed several times, or any problem originated from a detachment of the markers from the hand surface, experiments would need to be repeated. Moreover, regarding the inclusion of the hand model with EVE, the definition of this frame should be related to known physical points on the hand. In addition, the fact that the repeatable frame definition is based on physical landmarks keeps the mirroring property of the kinematic parameters of both hands. In order to accomplish this the proving tool was employed to select easily identifiable landmarks on the hand palm shown in figure 3.3. Similarly to the marker-based frame definition, two points where selected on the distal part of the hand, one lateral and another medial, and a third point was selected on a proximal part of the palm of the hand.

The repeatable frame vectors were defined following the same steps as the marker-based frame, in this case based on the landmark points. Any other point or vector expressed previously on the marker-based frame can now be transformed to the landmark-based frame.

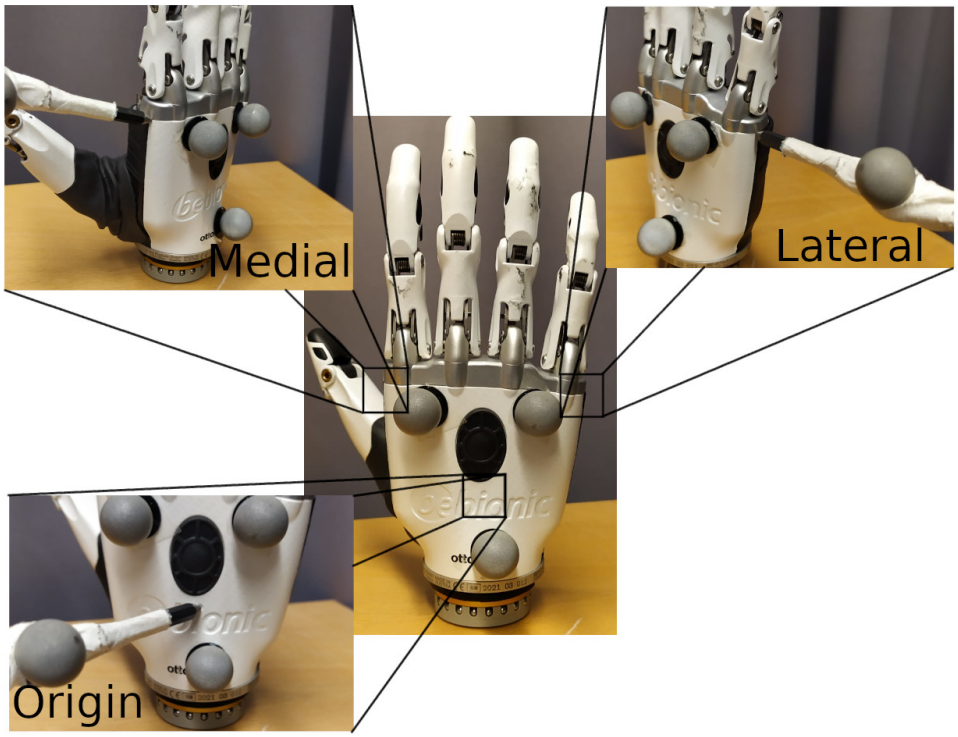

Figure 3.3: Landmarks for the repeatable frame definition

3.2.2 Multiple Marker Motion Capture

Motion captures of 40 seconds were performed per finger with a fixed sampling frequency of 100 Hz, where the fingers continuously performed motions of flexion/extension through their entire range of motion. Three markers were attached to each finger segment as depicted in figure 3.4. In order to be able to attach 3 markers to each finger segment a support structure had to be designed and 3D printed. The design of the 3D printer support is detailed in appendix C. The capability for the placement of 3 markers on each finger is an important feature for the analysis of the data. As performed in literature, and described in literature, the identification of each AoR and CoR should be performed actuating one joint at a time. However, due to the mechanical design of the BeBionic hand (fig. 2.2a, this was not possible to perform. In this case, the Kabsch algorithm was employed once more to describe the optimal rotation between the initial orientation of each finger segment, describing then a rotation matrix per segment, per frame. One of the three markers attached to each segment was designated as the origin of the frame, as it was a known position in the assumed rigid body. By this means, even if both finger segments were actuated at the same time during the motions, the relative rotations between segments were obtained. With the motion of each segment expressed on the frame of the previous link, the markers attached to the segment of interest would describe a circular motion around a static point in space, rotating around a moving point in space.

Once the AoR and Cor where computed for each segment, these where transformed back to the repeatable frame defined in the previous subsection.

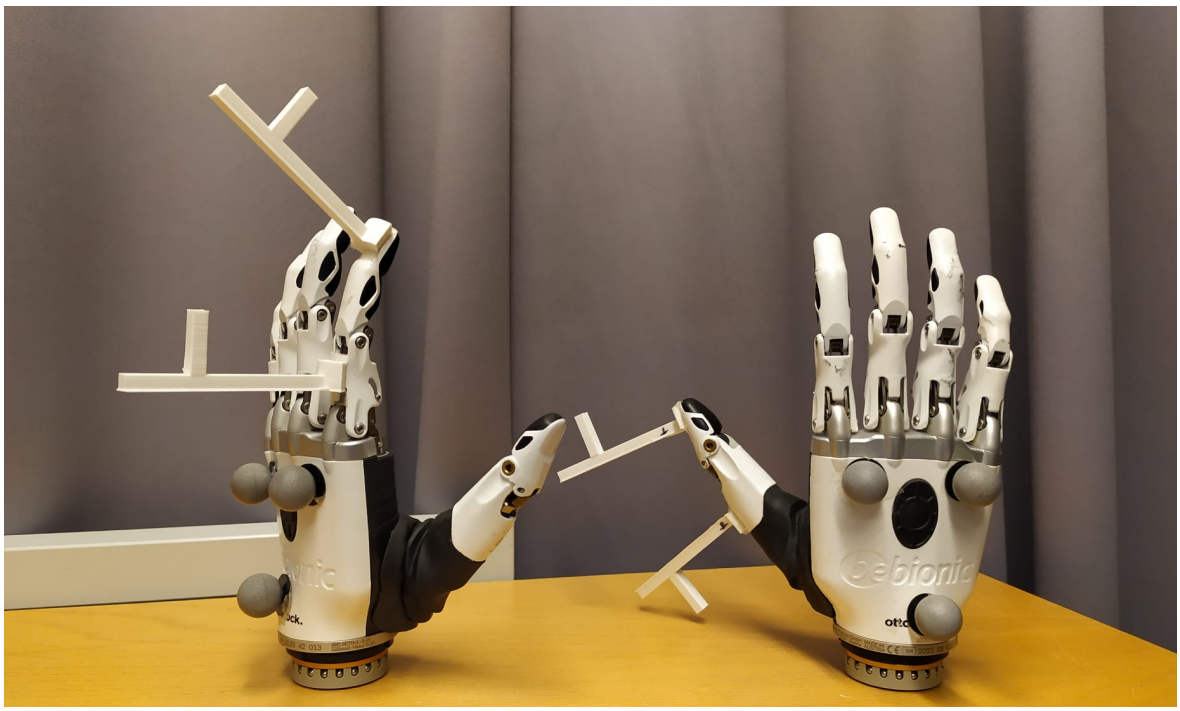

Figure 3.4: Designed support for the attachment of 3 points to each segment of the BeBionic fingers. These provide information on the absolute orientation of each segment at each frame. Different supports where created for the thumb and the other 4 fingers.

3.2.3 Dealing with Planar Motions: Proving CoR

As stated in [17], the concept of CoR cannot be applied to joints modeled as hinges. Even if for the problem being addressed the implementation to find the CoR is performed using the spherical fit cost function from [16], the markers attached to each finger show a planar motion. The solution of fitting a sphere to a set points describing a circular motion is infinite, as every point lying on the line described by the real CoR and the AoR is a solution for the fit. However, it is of interest to find a solution to find the approximate CoR of the joint, as it is needed to compute the forward kinematics of the BeBionic hand.

Based on visual inspection of the motion of the BeBionic fingers, it was determined that the CoR of each finger segment should be found between two screws shown in figure 3.5a. Using the probing tool described in 3.1, positional information of the location of the centre of these screws was gathered using the optical motion capture system as shown in figure 3.5b. The mean position between the probing of both sides was taken as an initial estimate of the CoR.

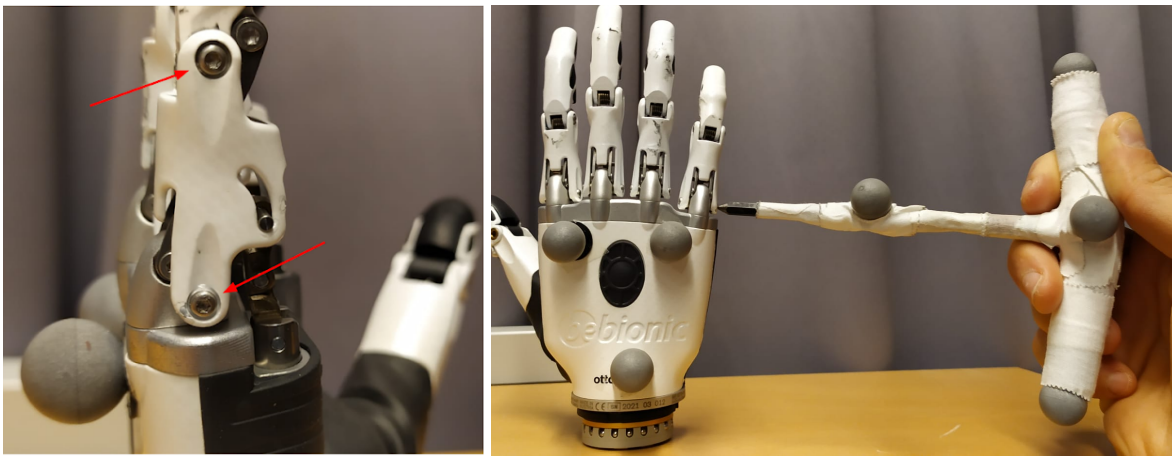

(a) (b)

Figure 3.5: (a) The red arrows point at the screws in between which the CoRs of both finger segments lie. (b) Probing of the CoR positions using the probing tool. Both sides of the finger were probed.

While this might be a solution for constraining the position of the CoR, the probed point might not lay on the line formed by the real CoR and the computed AoR. The probed CoR (supposedly near the real CoR) and the computed AoR and CoR (somwhere on the line formed by the AoR and real CoR) were combined. Given the line from the computed parameters using the methods described in appendix A, the projection of the probed CoR point on the line was computed, taking that as the estimated CoR. Figure 3.6 shows a representation of this approach where δ represents the assumed error in the final estimate of the CoR.

3.2.4 Surface Reconstruction

While for general robotics applications it is interesting to know the exact position of a single point, called the end-effector, in this case if is more interesting to know the position of a surface of contact with which the prosthetic hand will interact with the environment. The main approach followed for the reconstruction of the contact surfaces employed once more

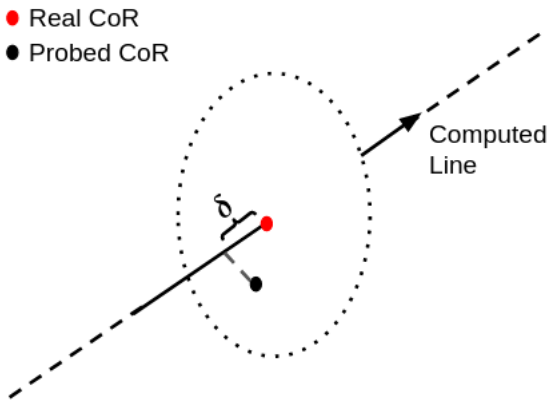

Figure 3.6: Schematic representing the computation of the estimate of the CoR from computed and probed values. The dotted cirlce represents the planar motion of the markers around the real CoR (red). The probed CoR (black) is projected on the computed line from the AoR estimate and the point laying on the line fromed by the AoR and the real CoR

the proving tool. With three markers placed on the palm of the hand and the set of markers of the proving tool, motion captures were performed while continuously sweeping the tip of the proving tool against the surface of interest. as it is shown in figure 3.7.

The point set obtained after the reconstruction of the prove over time, and transformed into the repeatable frame define a spatial distribution of points following the shape of the surface of interest. This non-uniform point distribution was then re-sampled using a voxel-based resampling method with a resolution of 5 mm. For the sake of the implementation in simulation software during further stages of the research conducted, a ball-pivoting triangulation algorithm [25] was exploited to generate geometric triangular mesh. The mesh generation algorithm provided meshes with small defects that were corrected with Blender [26].

(a) (b)

Figure 3.7: (a) Probing of the palm surface the white line shows an example of the path followed during the probing. (b) Probing of the finger surfaces, the white line shows an example of the path followed during the probing.

3.2.5 Kinematic Mapping

The objective of the kinematic mapping is to find the relation between the rotation of each segment on the underactuated fingers and the position measured by the encoder of each motor controlling each finger. It is worth mentioning that, while for later stages of this research it would be better to have a mapping between the motor angle and the finger angle, this information is not available from the BeBionic hands. As stated in chapter 1 the motor positional information from the hands has arbitrary units. The same set of motion captures obtained from section 3.2.2 was utilised for this purpose, as the encoder data was also captured from the ROS2 topics published by EVE. This data was obtained at a fluctuating frequency of around 100Hz. Both datasets were obtained asynchronously, as no synchronisation for external devices is provided by EVE, nor by the BeBionic hands. During the kinematic mapping implementation, the data had to be pre-processed. This pre-processing is covered in the following subsections.

Segment Flexion/Extension Angle Computation

The segment angle of rotation was obtained from the estimation of the rotation of each segment with respect to their corresponding previous segment on the kinematic chain. The *scipy.Rotation* library from python allowed to obtain the angle rotated about a certain axis (angle-axis representation of rotations). At each time step this magnitude was computed for which a relative rotation between segments was fully described.

Resampling of the BeBionic Data

The data obtained directly from the BeBionic through the EVE ROS2 interface showed an unstable sampling rate. To be able to compare the data from the hands with the external data obtained by the motion capture system, both were set to the same sampling rate. As both systems should theoretically provide data at the same sampling frequency, an estimation of the consistency of the sampling frequency for both signals was computed based on time differences of their timestamps. Afterwards, a resampling processing was applied to those signals showing big inconsistencies. The resampling was performed based on a simple linear interpolation between the provided values.

Synchronisation

Ideally, if a synchronization signal was used to start the motion capture system and the recording of the BeBionic hands data, when both signals would be plotted with their respective timestamps, there should be a certain degree of overlap between both signals. This overlap would be exact for a linear relationship between the encoder counts and the segment angles if both signals are scaled to an equal range. Since the signals where obtained asynchronously, a correlation analysis was performed in order to find the maximum similarity between both signals. This decision was taken under the assumption that the mapping would be quasi-linear based on signal visual inspection and prior knowledge on the type of mechanism transmitting the motion from the motor to the mechanism. From the correlation analysis, the time-shift between signals was extracted. Subsequently, the signals were cropped to the desired length taking into account the time-shift between them.

Mapping

With both signals of interest aligned based on the correlation analysis, their relation can be found. A least squares fitting technique was implemented to find the linear-on-the-parameters fit that approximates the relation between encoder counts and segment angle. This fit was implemented for both finger segments, for each finger, for each hand. Three polynomial cost function were fitted to the experimental data with increasing order, from 1st order to 3rd order as shown in the equations below. From the visualisation of the data, a higher order model might not provide any additional benefit. The polynomial with the best fit using RMSE as metric was selected as the kinematic map. Equation 3.4 shows the chosen polynomial functions, where N is the number of points to fit, y is the desired value and x is the input value for the mapping function. The values of a_i are the parameters to be estimated.

$$\frac{1}{N}\sum_{k=1}^{N}[y(k) - a_0 x(k) + a_1]^2 \tag{3.4}$$

$$\frac{1}{N}\sum_{k=1}^{N}[y(k) - a_0 x(k)^2 + a_1 x(k) + a_2]^2 \tag{3.5}$$

$$\frac{1}{N}\sum_{k=1}^{N}[y(k) - a_0 x(k)^3 + a_1 x(k)^2 + a_2 x(k) + a_3]^2 \tag{3.6}$$

3.2.6 Kinematic Model Validation

Generally, system models are validated with data obtained from the robot sensors, provided that the manufacturers calibrated the robot properly. This approach is used in [10]. However, no information about the BeBionic hands was provided, nor has been found in other sources, as it is a commercialised product with intellectual property rights on its design. Taking this premise as the starting point, a first assessment of the accuracy of the computed parameters was performed. Subsequently, a series of assumptions where utilised to try to evaluate which were the possible sources of error during the identification.

First, the trajectories of the markers attached to each of the finger segments were reconstructed using the computed forward kinematics, containting infromation from the AoRs and CoRs. The initial configuration of each of the three markers was found using the mean position for each marker during the first second of the motion capture. The difference between this mean position and the CoR of the segment to which the markers were attached was selected as the position of the marker in the segment's reference frame. The mean value was taken to prevent effects of noise in the definition of the initial configuration of the marker. The absolute distance from the measured markers to the reconstructed markers was computed and analysed.

This step of the validation provides information on the accumulated error due to errors in the estimation of the kinematic parameters of the hands. Although an absolute error for the parameters cannot be obtained, the comparison between the real trajectories of the markers and the computed trajectory encodes information about the total error accumulated for the computation of the positions of finger surfaces in space.

In order to find possible sources of error in this estimation, the first assumption made was

that both hands share a mirroring relation. This would imply that when two common features between both hands are aligned, the rest of the miss-aligned features would share the Cartesian coordinates in two axes but for the third axis, the sign of that component would be swapped. The definition of the repeatable frame described in section 3.2.1 effectively performs this alignment. Thus the CoRs found for each hand should share this property.

The second assumption made was that given two different motion captures, if the estimates of the CoR and AoR are reliably and consistently computed, those estimate should be the same when expressed in the defined repeatable frame. The same would happen for the landmarks defining the repeatable frame defined in section 3.2.1. The angle θ between the AoRs of each finger between two captures was computed with the intention of validating the computation of the AoRs following the geometric definition of the dot product:

$$\theta = arccos(\frac{AoR_{c1}\ AoR_{c2}}{||AoR_{c1}||\ ||AoR_{c2}||}) \tag{3.7}$$

Where AoR_{c1} and AoR_{c2} are the first and second motion captures computed AoRs of each finger and the operator $||\cdot||$ denotes the 2-norm of the vectors. In addition, the difference in position of the CoRs for two different motion captures of one hand, and the difference between the positions of the points defining the repeatable frame were computed.

The third assumption is that the axes of rotation of both joints belonging to one finger are the same, it is to say, both axes of rotation, even if originating from different points in space (different CoRs) should be parallel. This was defined out of intuition and observation of the physical hands. No further assumption can be done related to the axes of rotation of the hands, as there is no way of validating the absolute value of these axes of rotation. The angle between the AoRs of each joint were computed using the geometric definition of the dot product.

3.3 Dynamics Model Identification

The dynamic modeling of the BeBionic hands would try to represent the whole dynamics of each finger of the hand. As introduced in chapter 1, a simplistic 1D model may represent the dynamics of one of the fingers from the hands. Such an approach was taken in order to find the dynamic model of the BeBionic hands. Indirect current measurements, as well as indirect motor positions can be extracted from the BeBionic hands.

Even if these quantities have no physical meaning themselves, these are related to the actual values that determine the dynamics characteristics of the hands. While this is not ideal, it might be possible to use the indirect values extracted from the BeBionic hands to compute a dynamic model such that given indirect values of the position, velocity and acceleration of each finger, the indirect current values can be predicted. In such a scenario, the predictive model could be used to assess physical properties of external objects inside the hand after a calibration.

One of the main problems encountered during the modeling of the dynamic behaviour of the BeBionic hands is the dominance of the friction component. Based on the description of the hardware a high level of residual friction in the system was expected, as this is common in certain non-backdrivable systems [27] such as the BeBionic. The hard discontinuity of the real friction characteristics around $\dot{q} = 0$ increases the complexity of the parameter identification.

In order to avoid these discontinuities, it was decided that the dynamic model would be implemented for certain velocity values above a determined threshold. This decision also took into consideration the fact that the situations in which the information about the motor currents values are of high importance might be those during which the fingers are moving. During these situations, the motor currents are needed in order to detect any level of external resistance during a grasping tasks. Due to the non-backdrivable nature of the mechanism in the BeBionic hands the detection of objects present during grasping motions is crucial, in order to avoid damaging both the hardware and the object being grasped/manipulated.

In an attempt to provide sufficiently excitatory signals to the model, such that each of the model parameters shows predominance, a set of trajectories were programmed for the BeBionic to follow. A total of 12 movement where performed covering different speeds and ranges of motion for each finger.

First a full flexion extension motion at maximum speed was performed, followed by 4 motions divided into: closing until half of the range of motion, closing until the maximum limit of the range of motion, opening until half if the range of motion and finally opening to the initial configuration again, all these at max speed. The remaining 6 moves were the same reducing the velocity at half of it's maximum value. Due to the limited control available on the BeBionic hands, it is not trivial to generate complex signals that might induce a higher excitation of certain parameters of the dynamics of the hands. With the trajectories here described, the main excited parameters are the friction-related parameters and the spring component.

Data for the identification of the dynamic parameters was obtained through the EVE ROS2 interface and resampled to a 100Hz. During the resampling procedure, both the position and currents information where synchronised based on their timestamps in order to have information of both signals in the same moment in time.

3.3.1 Position Pre-processing and Velocity and Acceleration Computation

The position information obtained from the encoders of each finger of the BeBionic hands presents high values already in the initial configuration of the hand (open hand configuration). This number increases with the closure of the fingers. In order to avoid extreme values when computing velocities and accelerations from the available position information, the positions were re-scaled to a range from 0 to 100.

Next, the velocities and accelerations of the fingers were computed using discrete differentiation:

$$\dot{q_k} = \frac{q_{k+1} - q_k}{t_{k+1} - t_k} \quad , \quad \ddot{q_k} = \frac{\dot{q_{k+1}} - \dot{q_k}}{t_{k+1} - t_k} \tag{3.8}$$

The computation of these quantities based on finite differences is prone to the generation of noise when computed from encoder counts. Thus, the signals were fitlered offline with a 0 phase delay low-pass (6Hz) infinite impulse response (iir) filter.. The choice for the cutoff frequency was made based on the observation of the resulting filtered signals. With both signals filtered, the velocity threshold was applied, selecting only the components of all the signals (including the currents).

3.3.2 Model selection

Four models were chosen as candidate models for the identification. Each of the models was selected based on observation of the system behaviour and the mechanical design of the hands. First, a damper model was selected. Since the dynamic behaviour of the hands is highly determined by the friction in the system, it was hypothesised that the system could be represented with a term linearly related to the velocity:

$$\tau = b\ \dot{q} \tag{3.9}$$

Next, a linear spring-mass-damper (SMD) model was chosen. This model matches the mechanical design of the BeBionic finger, thus the system might be able to be represented as an SMD system:

$$\tau = m\ \ddot{q} + b\ \dot{q} + k\ q \tag{3.10}$$

The third model chosen was an extended version of the SMD model, in which an extra term is added with the intention to better represent the friction dynamics of the system. This term adds a constant torque to the system, and it's referred to as the Coulomb friction (F_c in equation 3.11). F_c depends on the sign of the velocity of the system, introducing a discontinuity on $\dot{q} = 0$. The modeling choice of utilizing dynamic data situations in which $|\dot{q}| > \dot{q}_{th}$ suppresses the non-linear effects of the discontinuity. The dynamics of this system are described by:

$$\tau = m\ \ddot{q} + b\ \dot{q} + F_c\ sign(\dot{q}) + k\ q \tag{3.11}$$

The last model chosen encodes a more complex behaviour of the system dynamics. This model introduces an extra term representing friction, in addition to the viscous ($b\ \dot{q}$ in equation 3.9) and coulomb friction terms. This extra term is a representation of the *Stribeck effect*. The Stribeck effect is described by the Stribeck curve characterised by equation 3.12 as described in [28].

$$(F_c + (F_s - F_c)e^{-|\dot{q}|/\dot{q}_s})sign(\dot{q}) + b\ \dot{q} \tag{3.12}$$

Here F_c represents the same term as in equation 3.11, F_s is the static friction and b is the viscous friction coefficient. The friction model considering the Stribeck effect is a highly non-linear model, effectively nonlinear on the parameters F_c, F_s and F_v. The friction force as a function of velocity with the taking into account equation 3.12 is represented in figure 3.8, choosing arbitrary values for the previously referred parameters, where a discontinuity on $\dot{q} = 0$ can be perceived.

To find the parameters that describe the friction dynamics of the Stribeck effect a non-linear optimization must be implemented. For the sake of simplicity, a different approach was proposed. Knowing the shape of the Stribeck curve when disregarding a range of slow velocities, it was hypothesised that a combination of two functions linear on the parameters could describe a similar behaviour as the one seen for the Stribeck curve. From figure 3.8 it can be seen that as velocity asymptotically approaches 0, the value of the force seems to increase according to the reciprocal of the velocity. For values of $\dot{q} = 0$ the force would be infinite, nevertheless, disregarding velocities near that point solves this problem while keeping part of the behaviour of the Stribeck curve. With increasing values for the velocity, the force seems to hold a linear relationship with the velocity. In addition, the extension of the linear region until the ordinate axis would reveal that for a $\dot{q} = 0, \tau \neq 0$. This phenomenon is due to the presence of the Coulomb friction component F_c and static friction effects.

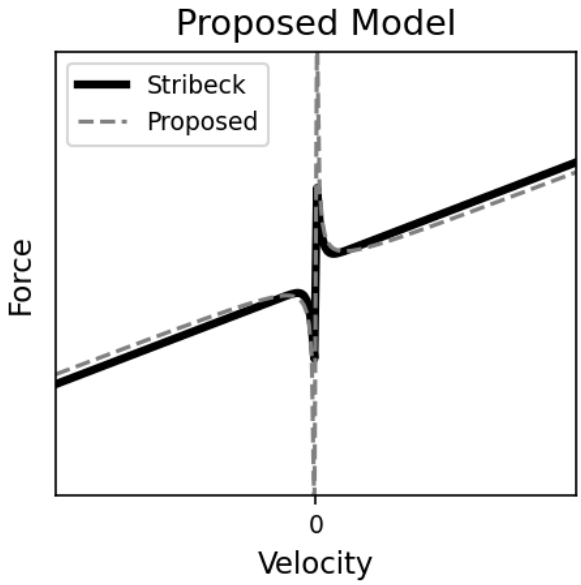

Figure 3.8: Stribeck curve shape based on equation 3.12 compared with the proposed model from equation 3.13

With all these observations in mind, the proposed model is a spring-mass-damper system in which the damper is divided into the viscous friction, the coulomb friction and a term proportional to the reciprocal of the joint velocity. The model is described by the following equation:

$$\tau = m\ddot{q} + b\dot{q} + F_c\ sign(\dot{q}) + F_{rec}\dot{q}^{-1} + kq \tag{3.13}$$

The proposed model shows a similar behaviour to the Stribeck model under the conditions imposed previously in this section. In addition, the model is linear on the parameters, for which there is no need to implement non-linear optimization techniques to solve for these parameters.

3.3.3 Parameters Computation

The estimation of the dynamic parameters for robotic systems was introduced in 1, it is a common practice amongst literature to generate an estimate of the dynamic parameters of linear systems using a LS approach. Each of the equations presented above can be expressed in a reduced form that comprises the currents, the motions and the parameters in three different arrays. As a generalisation this can be expressed as:

$$T = \Phi(\ddot{q}, \dot{q}, q, \dot{q}^{-1})\gamma \tag{3.14}$$

Where T is a $n \times 1$ matrix where n is the number of samples to be used. Φ is an $n \times k$ matrix where k is dependant on the model chosen. It contains information on the kinematic data gathered for the identification in its columns. Lastly, γ is a $kx1$ matrix containing the parameters to be found:

$$\begin{bmatrix} \tau_0 \\ \vdots \\ \tau_n \end{bmatrix} = \begin{bmatrix} \ddot{q}_0 & \dot{q}_0 & q_0 & \dot{q}_0^{-1} & sign(\dot{q}_0) \\ \vdots & \vdots & \vdots & \vdots & \vdots \\ \ddot{q}_n & \dot{q}_n & q_n & \dot{q}_n^{-1} & sign(\dot{q}_n) \end{bmatrix} \begin{bmatrix} m \\ b \\ k \\ F_{rec} \\ F_c \end{bmatrix} \tag{3.15}$$

Given the sufficient samples n this problem becomes an overdetermined system of equations that can be solved using LS:

$$\hat{\gamma} = (\Phi^T \Phi)^{-1} \Phi^T \, T \tag{3.16}$$

The best dynamic model able to describe the dynamics of the hand was selected by computing the RMSE between the unitless currents used to compute the model and the kinematic data used to find the dynamic parameters.

3.3.4 Object detection during grasping motions

Once the dynamic model selection and the parameter computation was performed, an experiment was performed to assess the capability of the hands of detecting an object during grasping tasks. During the experiment two objects with different material properties were placed in the hand during flexion/extension motions of the index finger.

The two objects selected for the experiment were a wooden cylinder and a cushion. It is apparent that both objects are defined by different material properties. The wooden cylinder is a stiff object, under the load of the hands closing, it will not show any kind of deformation, stopping the motion of the hands. On the other hand, the cushion is a compliant object, which will deform under the load of the hands during a grasping task.

During both grapsing tasks, the unitless currents values as well as the unitless position values for the hand were recorded. Afterwards, the position data was processed as described in section 3.3.1. Finally, the identified parameters were used to predict the currents of from the processed motion data. The measured unitless currents and the predicted ones were compared, in order to assess the potential of the hands for the detection of objects during grasping tasks.

Chapter 4

Results

This chapter provides an overview of the results obtained from following the methodology described in the previous chapter. Section 4.1 introduces the main result from the application described in chapter 3. Section 4.1.1 shows the resulting kinematic mapping for the BeBionic hands. Next, section 4.1.2 compares the measured marker trajectories from the motion captures with a forward kinematic reconstruction of these trajectories using the information from the previous sections.

4.1 Kinematic Modeling

The complete kinematic model for the BeBionic hands is fully described by the computed CoRs, AoRs and mappings from motor encoder counts to joint angles. It is usual to describe kinematic models to describe the pose of an end effector of the robot, in this case, represented as the contact surfaces rather than a single point in the finger. Figure 4.1 in combination with tables 4.1, 4.2, 4.3 and 4.4 provide a numerical and visual representation of a first part of the kinematic model of the BeBionic hands, all this data was obtained following the methods described in the previous chapter. Figure 4.1 provides a visualisation of the BeBionic hands in terms of the estimated CoRs, AoRs and contact surfaces points. On the other hand, the aforementioned tables show the computed values for these parameters for both hands.

Figure 4.1: BeBionic Hands kinematic model representation in original configuration. In this picture only one of the thumb positions is depicted.

Table 4.1: Left hand AoRs

Left Hand AoRs (m)				
Finger Joint		*X*	*Y*	*Z*
Thumb_1	Proximal	0.236	0.398	-0.885
	Distal	0.262	0.436	-0.860
Thumb_0	Proximal	0.034	0.997	-0.071
	Distal	-0.0001	0.999	-0.054
Index	Proximal	0.092	0.986	0.141
	Distal	0.113	0.988	0.102
Middle	Proximal	0.059	0.998	0.038
	Distal	0.065	0.997	0.045
Ring	Proximal	0.026	0.993	-0.112
	Distal	0.054	0.996	-0.076
Little	Proximal	-0.048	0.989	-0.133
	Distal	0.020	0.985	-0.170

Table 4.2: Right hand AoRs

Right Hand AoRs (m)		
X	*Y*	*Z*
-0.201	0.452	0.868
-0.283	0.413	0.865
0.034	0.996	0.084
-0.068	0.997	-0.022
-0.088	0.986	-0.139
-0.098	0.985	-0.141
0.009	0.997	-0.080
-0.038	0.999	0.015
0.030	0.999	0.026
-0.037	0.993	0.115
0.077	0.992	0.091
0.046	0.978	0.202

Table 4.3: Left hand CoRs

Left Hand CoRs (m)				
Finger Joint		*X*	*Y*	*Z*
Thumb_1	Proximal	-0.005	-0.024	-0.042
	Distal	0.040	-0.062	-0.050
Thumb_0	Proximal	0.001	-0.013	-0.049
	Distal	0.051	-0.019	-0.072
Index	Proximal	0.045	-0.027	0.004
	Distal	0.076	-0.033	0.005
Middle	Proximal	0.047	-0.009	0.009
	Distal	0.082	-0.015	0.018
Ring	Proximal	0.048	0.007	0.009
	Distal	0.081	0.006	0.017
Little	Proximal	0.045	0.027	0.004
	Distal	0.076	0.029	0.013

Table 4.4: Right hand CoRs

Right Hand CoRs (m)		
X	*Y*	*Z*
0.001	0.026	-0.044
0.047	0.060	-0.055
0.003	0.013	-0.051
0.050	0.012	-0.078
0.047	0.024	0.005
0.075	0.027	0.011
0.049	0.008	0.010
0.085	0.009	0.021
0.048	-0.007	0.009
0.082	-0.011	0.017
0.043	-0.026	0.005
0.073	-0.032	0.010

4.1.1 Kinematic Mapping

Data Resampling

The gathering of kinematic data revealed an undesired inconsistency on the sampling rate of the BeBionic hands. This inconsistency can be observed in figure 4.2a where a depiction of the mean sampling period T_s is shown in red. This sampling period is related to the sampling frequency by an inverse relation. The theoretical sampling frequency of the BeBionic hands is 100Hz, which would be equivalent to a sampling period of 0.01s, as it is the case for the motion capture system (Qualisys on the image). In this case the averaged sampling period for the BeBionic data was about 0.018s, almost doubled. This inconsistency prevents the utilisation of this data for correlation or mapping purposes. To correct for this the data was resampled to the desired sampling frequency of 100Hz using linear interpolation in between

missing values. The reconstruction of signal was effectively produced as it can be appreciated in figure 4.2b, as no apparent distortion of the original signal was introduced during the resampling procedure.

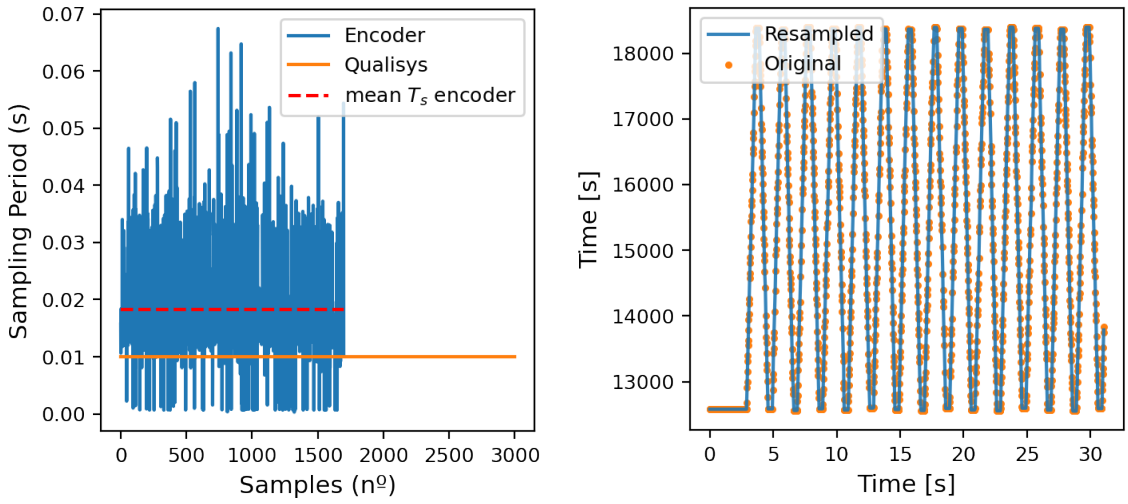

(a) (b)

Figure 4.2: (a) Unstability on the sampling frequency for the BeBionic hand when compared.(b) Resampled encoder signal (blue)

Synchronisation by Correlation

Due to the lack of availability of a synchronization signal between the motion capture system and the BeBionic hands a noticeable mismatch in time was present as it can be seen in figure 4.3. To correct for this misalignment a correlation based synchronisation was performed. This decision was made based on the observation of the signals to be synchronised, as the relation between them seems to be quasi-linear. The correlation analysis returned the correlation coefficients related to the similarity between signals, as well as the discrete time-shift at which this maximum correlation appeared. With this information, all the involved signals were shifted and trimmed to the adecuate lenght, resulting in a perfect alignment between the signals as it can be appreciated in figure 4.3

Function Mapping

The kinematic mapping was performed on the 5+1 fingers for each hand and each segment, where three polynomials where evaluated as candidate functions to find the linear-in-the-parameters relation between the encoder counts output by the BeBionic hand and the finger flexion/extension degree. These functions where linear, quadratic and cubic on the encoder counts. Tables 4.5, 4.6, 4.7 and 4.8 show the evaluation of the parameters found on the data gathered during the motion capture trials. In all of the case the cubic function show a better fit to the data provided, in some cases being close to the cuadratic function fit, especially for the thumbs.

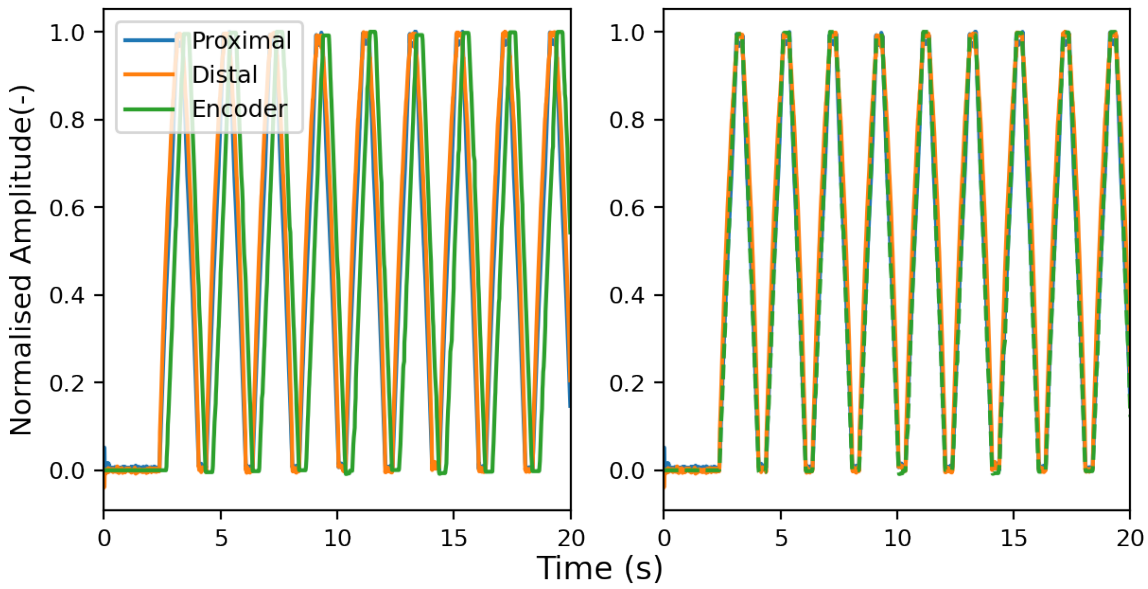

Figure 4.3: Signal alignment based on correlation analysis between the encoder values obtained from the BeBionic hands and the computed angle of flexion/extension of the finger segments.

Table 4.5: Result for the kinematic mapping fit from encoder counts to proximal segment angle for the right hand.

RMSE Right Hand Proximal Mapping (deg)			
Finger	*Linear*	*Quadratic*	*Cubic*
Thumb_0	0.546	0.402	0.383
Thumb_1	0.789	0.732	0.732
Index	1.230	1.141	0.948
Middle	1.690	1.163	1.129
Ring	1.653	1.210	0.991
Little	1.410	1.061	0.799

Table 4.6: Result for the kinematic mapping fit from encoder counts to distal segment angle for the right hand.

RMSE Right Hand Distal Mapping (deg)		
Linear	*Quadratic*	*Cubic*
0.988	0.622	0.606
0.986	0.848	0.848
4.418	1.261	0.990
3.109	1.457	1.199
3.786	1.311	1.098
4.021	1.475	1.089

Table 4.7: Result for the kinematic mapping fit from encoder counts to proximal segment angle for the left hand.

RMSE Left Hand Proximal Mapping (deg)			
Finger	*Linear*	*Quadratic*	*Cubic*
Thumb_0	0.579	0.487	0.476
Thumb_1	0.829	0.678	0.669
Index	1.496	1.189	0.979
Middle	1.624	1.432	1.299
Ring	1.374	0.958	0.875
Little	1.853	1.365	1.234

Table 4.8: Result for the kinematic mapping fit from encoder counts to distal segment angle for the left hand.

RMSE Left Hand Distal Mapping (deg)		
Linear	*Quadratic*	*Cubic*
0.659	0.647	0.645
0.796	0.756	0.752
3.236	1.119	1.016
3.184	1.427	1.294
3.399	1.459	0.980
3.351	1.513	1.335

Figure 4.4 shows a graphical representation of the mapping functions for four different fingers and one segment per finger. There it is possible to appreciate and understand the fact that all of the residuals after computing the RMSE for the kinematic mapping are really close. For both segments of the thumb it is almost impossible to appreciate any difference between the 3 models fit. A similar situation occurs with the proximal segment. However, when looking at the distal component, a slight curvature can be detected which is responsible for the sudden increase on the RMSE of the linear mapping.

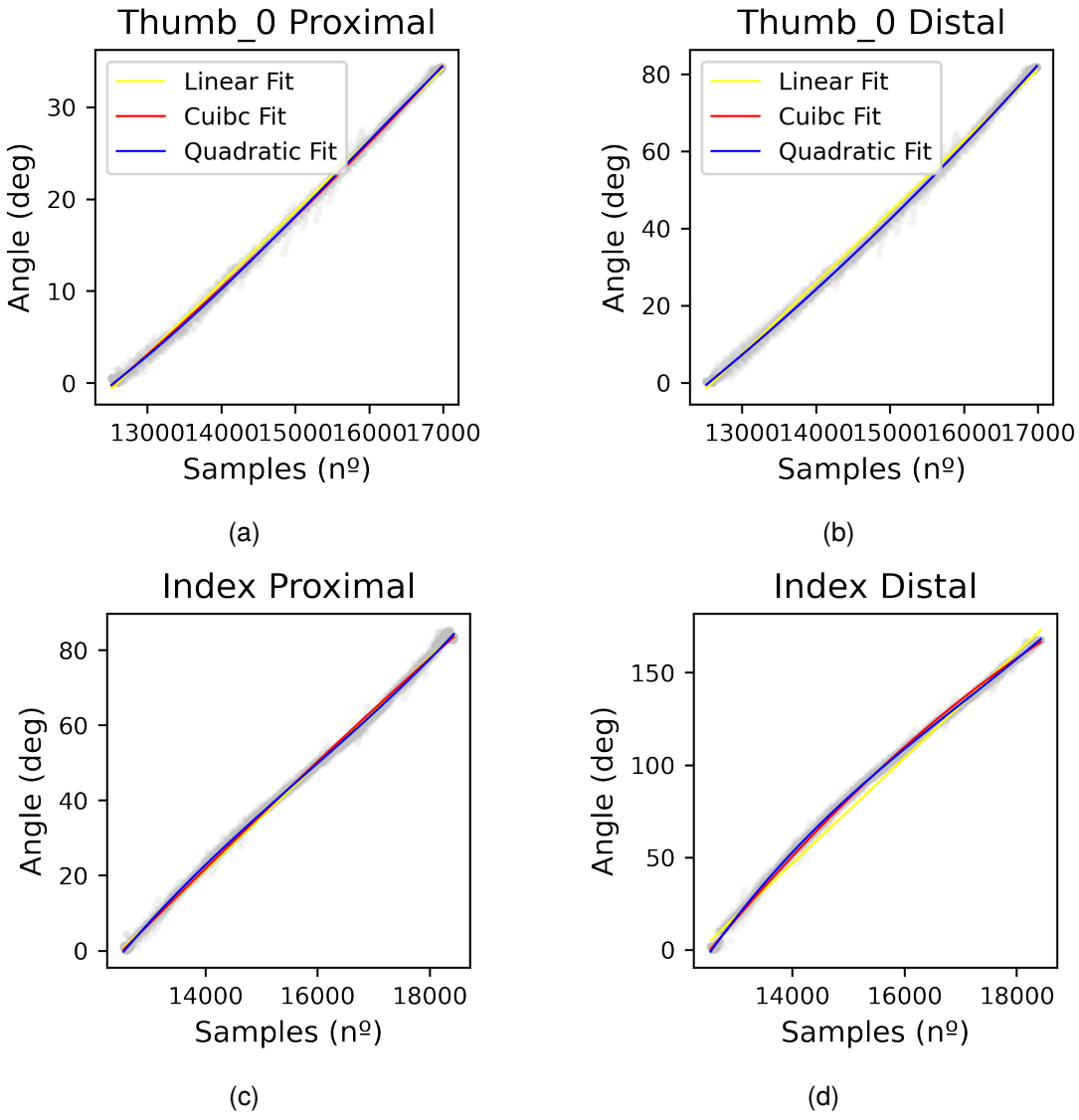

Figure 4.4: Fitting of mapping functions from unitless positions (encoder counts) to segment angles. (a) Shows the mapping for the thumb proximal segment. (b) shows the mapping for the thumb's distal segment. (c) Shows the mapping of the index proximal segment. (c) Shows the mapping for the index distal segment.

4.1.2 Marker Trajectory Reconstruction

In order to reconstruct the position of the markers the forward kinematics of all the markers attached to each finger segment. The absolute distance between the reconstructed markers and the measured markers was calculated to assess the validity of the kinematic parameters obtained.

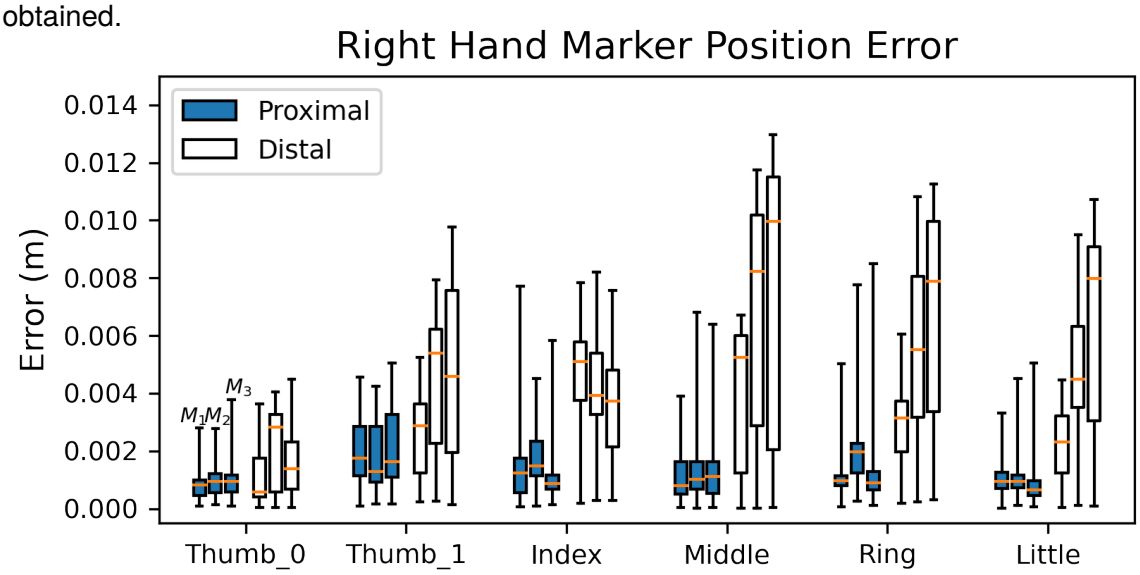

Figure 4.5: Right hand error plots. Box plot figure showing in blue the error distributions for the markers attached to the proximal segment.M_1, M_2 and M_3 correspond to each of the markers attached to each segment during the motion captures . In white, the error distributions for the markers attached to the distal segment. These errors were computed per finger.

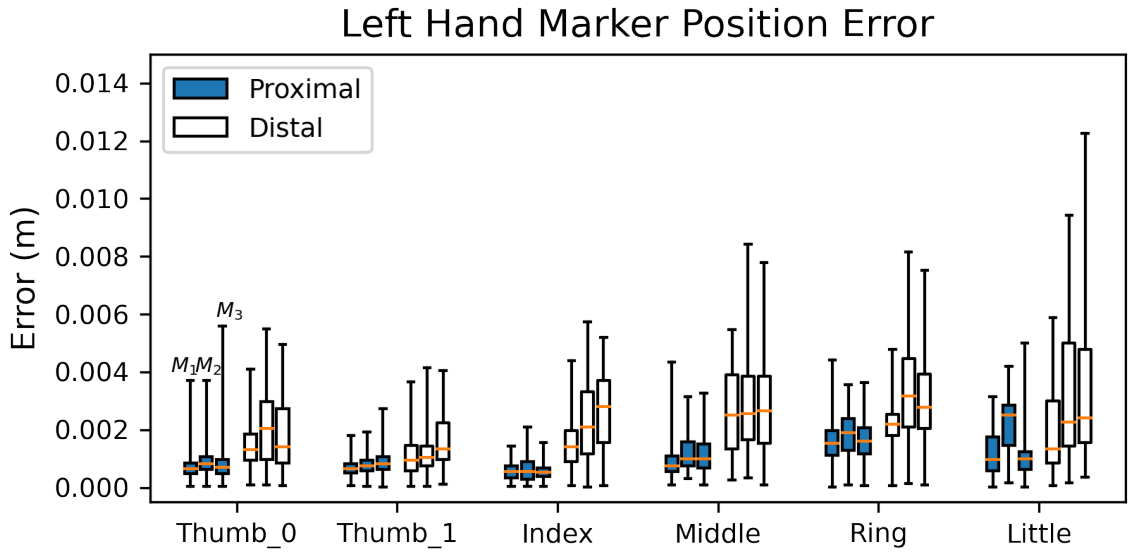

Figure 4.6: Left hand error plots. Box plot figure showing in blue the error distributions for the markers attached to the proximal segment.M_1, M_2 and M_3 correspond to each of the markers attached to each segment during the motion captures . In white, the error distributions for the markers attached to the distal segment. These errors were computed per finger.

Figures 4.5 and 4.6 represent the distributions of the errors per finger, per segment. The y axis encodes the magnitude of the error, while the x axis encodes which finger is being studied. In blue, the distributions for the errors of in the predicted trajectories for the proximal segments are shown. In white, the errors for he predicted trajectories of the distal segments of the fingers are presented. The median values of the distributions are represented by the orange horizontal lines. The whiskers span thw whole range for the values of the error. The tags M_1, M_2 and M_3 denote each of the markers attached to the finger, following the same order for the distal segment box plots.

Both segments for each finger show skewed distributions, with the distal segment showing consistently higher absolute errors compared to the errors presented by the proximal segments. This is the situation for both hands. In addition, the interquartile range increases substantially for the error distribution of the distal segment compared with the proximal segment of the same finger. A noticeable difference is appreciable between the left and right hand models, with the right hand showing higher levels of error in all cases or both segments, for all the fingers.

It is of special interest the case of the middle finger of the right hand, where not only the highest error levels are present, but also the biggest differences between the median values of the distributions are shown, as for example the median value for the error of the M_3 proximal marker changes from approximately 1 mm for the proximal segment, to almost 1 cm for the distal segment.

On the contrary, for the left hand, fingers such as the thumb in both of its configurations show a lower increase both in median and interquartile range staying at errors below 2mm. Nevertheless, a similar behaviour as the one described by the middle finger of the right hand, the little finger of the left hand shows higher maximum error and upper quartile limit values.

4.1.3 Kinematic Model Assumtions

Three main assumptions were made by observing the mechanical design of the BeBionic hands. The computation of this metrics, rather than providing a pure validation of the identification, tries to reassure assumptions made in section 3.2.6 that will be used in the discussion of this work.

The first assumption made was with respect to an expected mirroring property between the hands, where CoR coordinates should have the same components in two axes, while for the third the sign should be reversed. It can be deduced from tables 4.4 and 4.3. The observation of the points in those tables show a relative similarity between the CoRs for both hands, with the distinctive feature that the Y coordinate between points, even if not with the exact same absolute value, its sign is inverted. The implications that all these findings might have in the validity of the kinematic model is discussed in the next chapter.

The second assumption made was regarding the repeatability of the kinematic parameters found for two different motion captures. The frame repeatability computations was performed between two motion captures for the left hand. All of the landmark features used to define the repeatable frame where transformed to that same frame for two different captures with two different marker configurations. No difference was found between the resulting positions of the proved landmarks, proving that the repeatable frame is reliably defined and computed.

The repeatability on the computation of the AoRs and the CoRs was computed from the same motion captures, using as metrics the angle between axes of rotation and the distance be-

tween CoRs. The resulting values for the repeatability check can be found in tables 4.9 , 4.10 and 4.11. As for the AoRs, the deviation was scattered between a maximum of 6.87 degrees for the proximal joint AoR deviation between captures, and a minimum of 0.912 degree for the distal joint AoR deviation, with means of 3.87 degrees and 3.75 degrees respectively for the proximal and distal joints. As for the CoR, a maximum deviation of 6 mm and a minimum of 0.2mm deviations were found during the computation of the repeatability. The average difference between computations of the CoRs in different captures is of 2 mm.

Table 4.9: Difference between the computed AoRs for two captures

AoR Repeatability (deg)						
Finger Joint	*Thumb_0*	*Thumb_1*	*Index*	*Middle*	*Ring*	*Little*
Proximal	6.857	4.580	2.88	3.887	4.005	1.020
Distal	5.275	5.044	0.911	2.130	4.172	5.020

Table 4.10: Difference between the computed CoRs for two captures

CoR Repeatability (m)				
Finger Joint		*X*	*Y*	*Z*
Thumb_1	Proximal	-0.006	0.002	0.000
	Distal	-0.005	-0.001	-0.002
Thumb_0	Proximal	-0.002	0.003	0.003
	Distal	-0.003	0.001	0.004
Index	Proximal	-0.002	-0.002	-0.001
	Distal	0.002	-0.001	-0.008
Middle	Proximal	0.001	0.000	0.000
	Distal	0.000	-0.003	0.001
Ring	Proximal	0.000	0.002	0.001
	Distal	-0.001	-0.002	-0.001
Little	Proximal	-0.002	-0.000	0.001
	Distal	0.003	-0.001	0.002

In addition, the angle between the joints for a single motion capture was computed. Similar results were found when compared to the deviation betwen captures, with a maximum deviation of around 8.45 degrees and a minimum deviation of 0.55 degrees. In this case, however, the mean deviations differed by 3 degrees, with a mean deviation of 5.55 degrees for the right hand, and a mean deviation of 2.5 degrees for the left hand.

Table 4.11: Angle between the AoRs of consecutive joints for all the fingers of the left hand

Deviation Between Joint AoRs (deg)						
Hand	*Thumb_0*	*Thumb_1*	*Index*	*Middle*	*Ring*	*Little*
Right	5.191	8.456	0.552	6.103	6.434	6.624
Left	3.024	2.194	2.553	0.583	2.613	4.430

4.2 Dynamic Modeling

4.2.1 Model selection and Parameter computation

Four dynamic models where selected to be fit to the gathered data for all the fingers. Figures 4.7 and 4.8 show the performance of the four models under the conditions described in chapter 2. Figure 4.7 shows the data fitting for the right thumb finger, while figure 4.8 shows the data fit for the right index. As it can be seen, the currents profiles show different behaviours for these fingers, with the rest of the fingers showing similar profiles to the index. In blue, the gathered data is shown, in orange, the resulting unitless currents predicted by the fitted model are displayed. The top left plot shows that the damper model performs poorly and inconsistently for both fingers, revealing that the model is too simple to be able to capture the dynamics of the system. Next, on the top right part, the fitting of the SMD system is shown. The components present in this model match exactly with the mechanical design of the BeBionic hands. It is clear form the plot, that the SMD system is not capable of capturing the dynamics of the system even if it might have features similar to the mechanical design of the hands. The performance of the SMD system is similar to that of the D system, overshooting lower current values and underestimating higher current levels. The bottom plots show the fittings for the friction-extended models. The bottom left plot shows the fits for the system extended with the Coulomb friction term (SMD + F_c), and the bottom right plot shows the system described by the proposed model to represent part of the Stribeck effect (SMD + F_{rec} F_c). Both systems seem to provide accurate estimates of the unitless currents obtained from the BeBionic hands. Nevertheless, the computation of the RMSE of the error of between signals consistently shows that the SMD + F_{rec} F_c provides better fits for the data. The RMSE for the fit is shown in tables 4.12 and 4.13

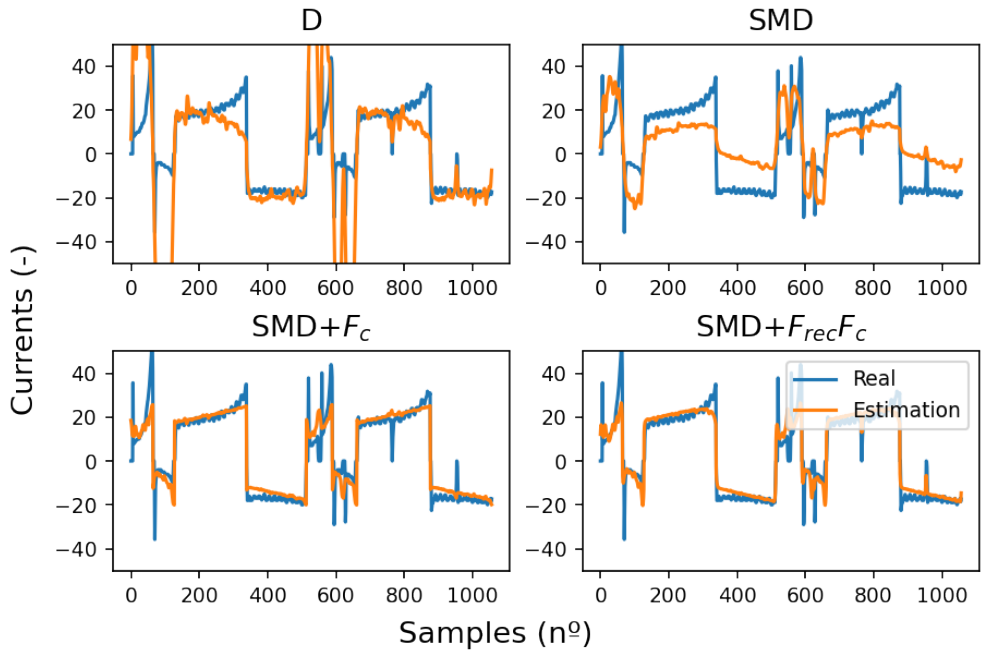

Figure 4.7: Dynamic models fit to the unitless currents data for the right thumb. On blue the real data obtained from the BeBionic. On orange the estimation performed per model. Four models are presented, damper model (top left), spring-mass-damper model (top right), spring-mass-damper + Coulomb Friction (bottom left) and spring-mass-damper + Coulomb Friction + Reciprocal Force (bottom right).

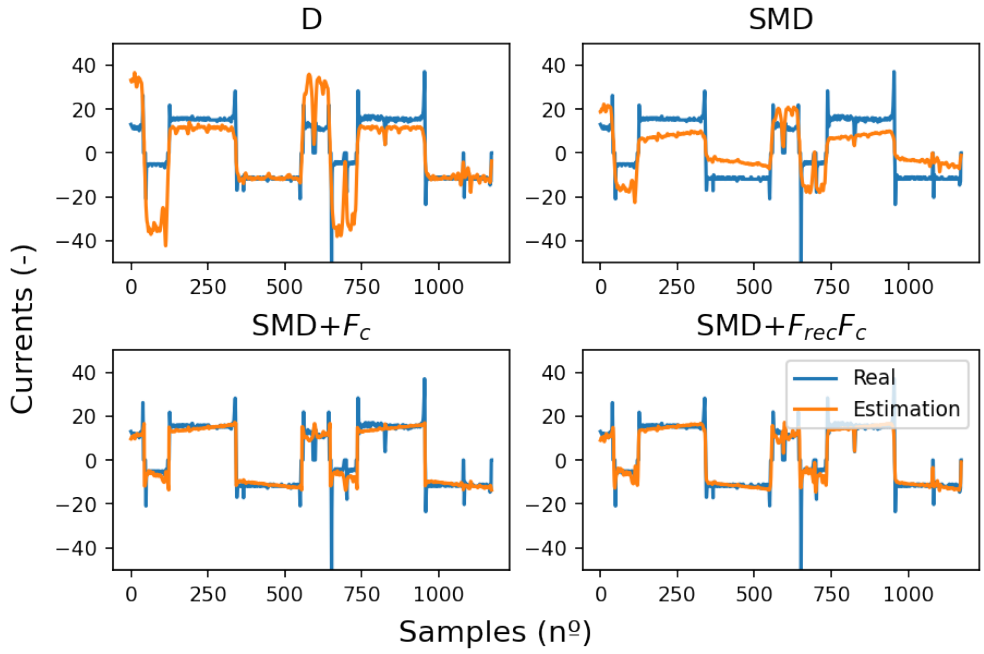

Figure 4.8: Dynamic models fit to the unitless currents data for the right index. On blue the real data obtained from the BeBionic. On orange the estimation performed per model. Four models are presented, damper model (top left), spring-mass-damper model (top right), spring-mass-damper + Coulomb Friction (bottom left) and spring-mass-damper + Coulomb Friction + Reciprocal Force (bottom right).

Table 4.12: Predicted Currents RMSE for the right hand

Predicted Currents RMSE Right hand				
Finger	D	SMD	SMD + F_c	SMD + F_{rec} F_c
Thumb	27.624	18.653	13.407	12.872
Index	23.671	18.157	12.393	11.251
Middle	19.520	16.899	13.041	11.165
Ring	10.803	10.449	10.292	10.264
Little	20.448	, 17.727	14.311	12.863

Table 4.13: Predicted Currents RMSE for the left hand

Predicted Currents RMSE Left hand				
Finger	D	SMD	SMD + F_c	SMD + F_{rec} F_c
Thumb	29.31	20.830	15.536	14.793
Index	20.103	17.071	13.132	11.714
Middle	19.719	16.940	13.025	11.154
Ring	20.033	17.234	13.443	11.687
Little	20.874	18.109	14.579	13.108

4.3 Object detection during grasping motions

Figures 4.9a and 4.9b show the comparison between the predicted unitless currents and the measured unitless currents given the computed parameters for the proposed dynamic model. Figure 4.9a shows the comparison between signals when interacting with a stiffer object. A sudden rise in the current values can be seen for the measured unitless currents, compared to the predicted ones. Quickly after the current rise, the safety hard-coded current limit for low velocities is activated stopping the motion of the finger. On the other hand, figure 4.9b shows the predicted signals when interacting with a compliant object. A similar measured signal increase is presented, however in this case, even if the current has risen, the current limit for low speeds is not reached as the finger is able to deform the object and move.

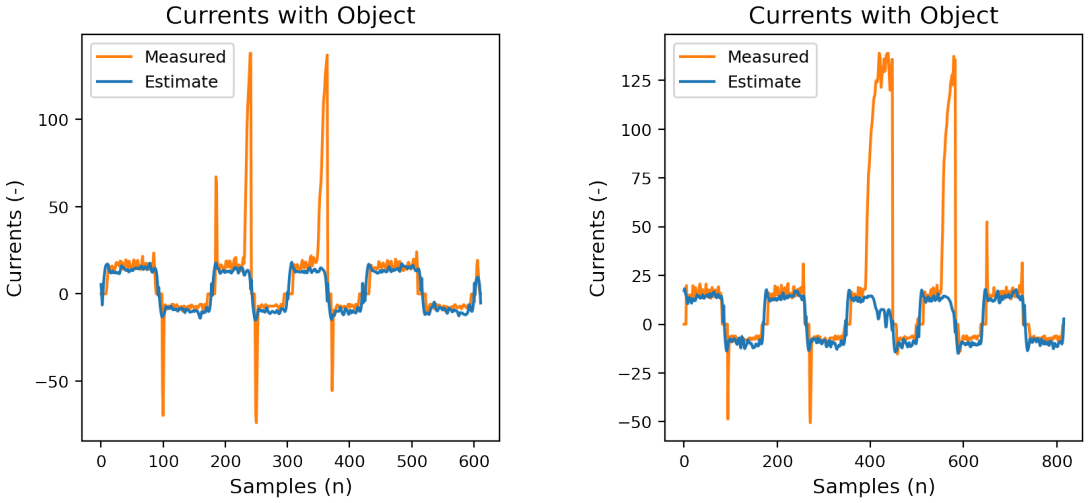

(a) (b)

Figure 4.9: (a) Predicted currents compared with measured currents during grasping of a stiffer object. (b)Predicted currents compared with measured currents during grasping of a compliant object. On orange, the measured unitless currents, on blue the predicted unitless currents.

Chapter 5

Discussion and Conclusion

The presented work describes the data gathering and processing for the development of a kinematic and dynamic model of a pair of robotic hands, in this case, the BeBionic hands. This section aims to provide an analysis of the main findings of the presented work, and discuss the points in which it can be improved. This section is divided in three parts.

The first part provides a response to the first research question set out. It summarises the methodology followed and the results obtained for the implementation of the kinematic parameter identification techniques described in section 4.1. At the same time, the validity of the results is discussed, providing an in depth analysis of the findings. In addition, the limitations of the implemented methodology are discussed. The second part provides a response for the second research question. It covers an analysis similar to that of the first part, but for the findings from the implementation of the dynamic parameters identification techniques described in section 4.2.

Finally, a general conclusion is presented regarding the adequacy of the BeBionic hands for their intended purpose in the presented framework. A set of recommendations and possible research lines following this work are proposed in order to extend the capabilities that the BeBionic hand can provide as manipulators.

5.1 Discussion on the Kinematic Identification

RQ1: Can we use motion capture data to derive a kinematic model of the BeBionic robotic hands?

A kinematic model of the BeBionic hand was successfully developed by finding all the necessary parameters for the description of the configuration of the hands in space from motion capture data.

First a motion capture protocol was developed and followed to gather information about the motion of the hands. Afterwards, identification techniques were implemented to extract the kinematic parameters of interest (AoRs, and CoRs) for both robotic hands.

A reference frame was defined at the palm of the BeBionic hands, so that the motion of each finger could be expressed with respect to the palm of the hand. A set of physical landmarks on the palm of the hand were chosen to define a consistent reference frame for different motion captures. The consistency on the definition of this frame in different motion captures

was assessed in section 4.1. For different motion captures, the positions of those landmarks expressed in the repeatable frame was the same.

Next, the AoR and CoR estimation algorithms described by [17, 16] were implemented. The estimation of the CoR provided inconsistent results due to the motion of the data gathered. This was solved by the utilisation of the proving tool described in 3.1. The proving tool constrained the position of the computed CoR to a realistic, consistent position. The consistency of the computation for the CoR was addressed in section 4.1.3, where the computed position of the CoRs for two different motion captures shows minimal deviation, with a maximal deviation of 6 mm for the thumb proximal CoR. In addition, it was hypothesised that both hands share a mirrored relation, proven also in 4.1.3.

Furthermore, the relation between the information available form the BeBionic hands and the configuration of the hand fingers was extracted and evaluated. Three polynomial functions were fitted to the data. The fitting showed that the relation between the unitless position form the BeBionic and the finger configuration hold a linear-in-the-parameters cubic relationship as shown in section 4.1.1. The mapping function found showed residual errors from ranging from 0.6 deg to 1.2 deg maximum. The mapping parameters were computed using the whole dataset gathered. This could lead to overfitting of the mapping function. In order to prevent overfitting, the dataset should be divided into smaller subsets to test that the parameters can properly infer the angle of the finger segment from the unitless position data.

Finally, the kinematic model obtained from the CoR and AoR values was validated. The trajectories of the markers attached to the fingers during the motion captures was reconstructed using forward kinematics, using the segment angles computed during the captures. The error between the computed trajectories and the measured trajectories was computed and displayed in section 4.1.2 in the form of box plots. The results for the kinematic reconstruction shows different error distributions per finger for each hand. The right hand consistently showed larger errors when compared with the left, especially for the distal segments. Part of the error for the distal segment is a consequence of the error propagation in the computation of the forward dynamics. The errors for the right hand showed up to 1 cm deviation as it is the case for the right middle finger, with this value being inside the inter quartile range. For the left hand maximum errors of around 5 mm were found to be inside the inter quartile range.

The main sources of error for the reconstruction of the marker trajectories are the computed parameters, in combination with possible inaccuracies when computing the joint angles from the motion capture data. It seems unlikely that the computed segment angles from the motion capture data proves to be the main source of error, as the same angles and ranges of motion were found for the same fingers of both hands. While the accuracy of the computed angles cannot be completely assessed, it is unlikely for the same fingers of different hands to show such an error difference for similar segment angles.

The contribution of the computed CoR to the error in prediction is also unlikely to be the source of such errors. The positions of the CoRs in each hand's reference frame share a mirroring property. Thus for similar the same fingers for both hands, the error introduced by the position of the CoR is expected to be similar, as the markers were placed at a similar distance from their respective CoR.

The contribution of a wrong estimation of the AoR seems the main source of error. This can be deduced from the comparison of the kinematic data between the left and right hand. Figures 5.1b and 5.1a show a high level of noise and data distortion in the capture data for the right hand compared with the left hand. The presence such noise in the data might be the cause of a wrong estimation of the AoR.

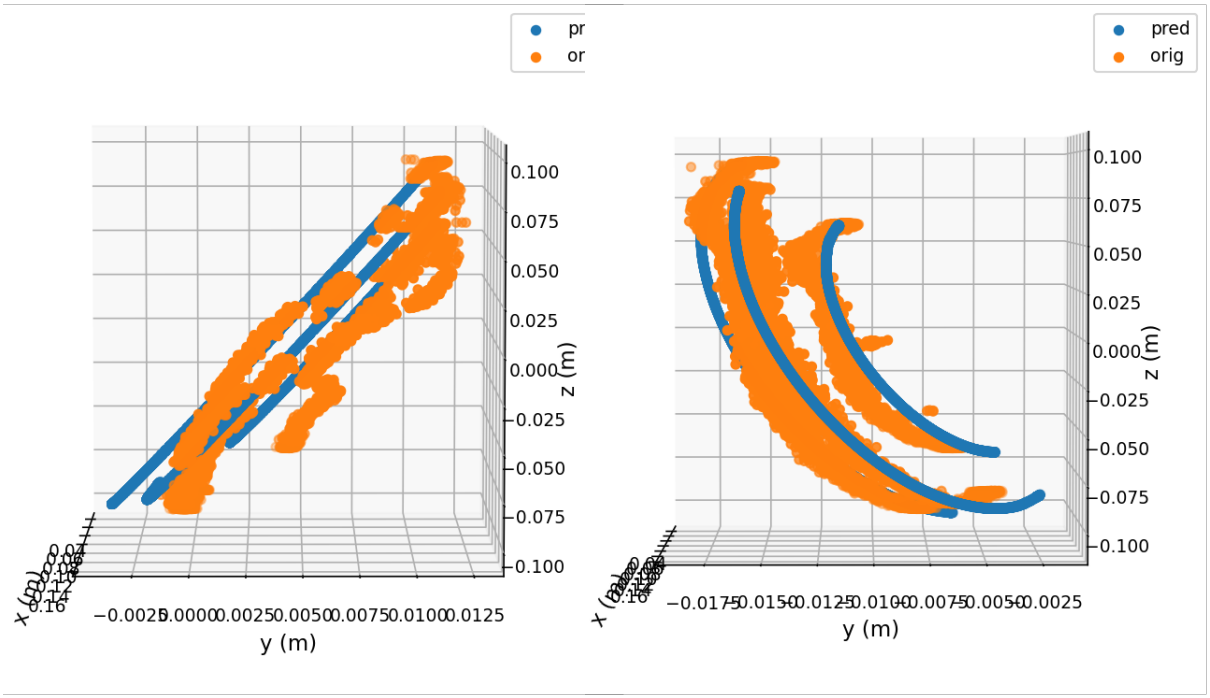

(a) (b)

Figure 5.1: (a) Scatter plot for the distal marker trajectories of the right hand. (b) Scatter plot for the distal marker trajectories of the left hand. For both, blue shows the reconstructed trajectory, orange shows the measured trajectory.

The inspection of the rest of the trajectories, show similar relations in term of noise between fingers of the right and left hand. This argument would be supported by the hypothesised relation between AoRs of joints of the same fingers. Recalling from section 4.1.2, it was hypothesised that the AoRs of joints in the same finger are parallel. Revisiting table 4.11, it can be seen that the difference in angle for the joints of the left hand is generally smaller than for the right hand. While this relation cannot be assured, it might exist between both metrics. In order to assess if this is the actual reason for the larger error for the reconstruction of the marker trajectories of the right hand, new data should be obtained and processed if needed in order to reduce the level of noise.

On the other hand, the methodology chosen for the estimation of the axis of rotation assumed that the markers performed a pure rotation around a circle. This algorithm was selected due to its simplicity and apparent robustness. However, having seen the amount of noise present in the data, a sensible approach would be to utilise the previously discarded method developed by Chang and Pollard [18]. There, Chang and Pollard argue the methodology they developed provides consistent estimations of the dominant axis of rotation for a hinge joint, even in the presence of a secondary axis of rotation as a source of noise. It would be interesting to see if their implementation would provide better estimates for the case of noisy data as the one presented in figure 5.1a.

The maximum error in the position estimation of the BeBionic fingers can be considered high taking into account the width of the surfaces of contact of the fingers.

5.2 Discussion on the Dynamics Identification

RQ2: Is it possible to compute a unitless dynamic model that can predict a force-related signal on the BeBionic hands, such that it is possible to distinguish the presence of objects interacting with the hands during grasping tasks?

A unitless dynamic model was successfully developed by finding a set of parameters that are able to predict the unitless currents in the motors of the hands, given motion data from the motors. The implemented model shows potential for the detection of objects, and properties of those, by comparing predicted unitless currents with measured ones.

First, unitless motor positions data and unitless motor currents data was gathered and processed for different hand configurations and motions. From the unitless positions of the motor, unitless velocities and accelerations were computed. Four linear-on-the-parameter models were chosen as candidates to represent a simplified estimation of the motor dynamics. The first two selected models were a damper-dominated (D) system and a spring-mass-damper system (SMD). A third model was an augmented spring-mass-damper (SMD +F_c) system with an additional constant term representing the Coulomb friction. Finally a fourth model was proposed in which a term reciprocal on the velocity of the system was added, with the aim to approximate the dynamics of the Stribeck curve (SMD +F_{rec} F_c).

The main problem for the implementation of such models are the non-linearities shown by the friction dynamics in section 3.3.2. In order to suppress these effects, it was proposed to describe the dynamics of the hands for velocities higher than a certain threshold. As described in section 3.3, the situations in which the motor is in motion is when the information of the unitless currents is of most relevance, as this provides information on the presence of objects in the hand.

The four models where fit to the data using an LS fit as described in section 3.3.3, with the SMD + F_{rec} F_c producing the smallest RMSE for all the fingers. It is important to state that the proposed model is an approximation of the real dynamics of the system, and more complex models should be implemented to describe the dynamics of the BeBionic hands more accurately. Furthermore, the literature study revealed that it is relevant to compute optimal trajectories for the identification of system dynamics. These trajectories are optimized to excite frequency ranges in which all the parameters of the model show predominance. Although following this approach might provide a better insight on the dynamics of the BeBionic hands, it would be hard to implement. The control capabilities for the hand are limited, as well as the actual physical information necessary for the optimal trajectory planning and tracking.

Even if the proposed model can predict the unitless currents during finger motions, the proposed modeling choices were supposed to suppress the effects of static friction, however these effects (or small portion of those) are still present in the data. As it can be seen in figures 4.7 and 4.8, current spikes at the beginning of each motion performed are still present, and not predicted by the proposed model. This could be solved by increasing the selected velocity threshold, nevertheless, it would have a negative effect on the detection of objects during grasping motions.

Regarding the detection of objects in the hand during grasping motions, an experiment was performed in which two different objects where placed in the hand during flexion/extension motions of the index finger. Figures 4.9a and 4.9b show the unitless current profiles for grasping tasks with stiff and compliant objects respectively. Based on the observation of the

plots, the representation of the dynamics of the BeBionic hands with the proposed model shows the potential of being able detect the presence of objects during grasping tasks. In addition, if a calibration is performed, the BeBionic hands might be able to identify material properties of the objects such as their stiffness.

Finally, the potential implementation of the object detection and object properties identification is however jeopardized by the limited bandwidth of the current measurements. The sampling frequency of the unitless current values is 100 Hz, which could potentially be too slow for the manipulation of fragile objects, as small increases in stress over, for example, gas vials could easily break them.

5.3 Conclusions & Future work

The BeBionic hand is a suitable prosthesis for the day to day utilisation of human beings, it is robust, intuitive and provides an extensive range of grips restoring lost functionalities. Some of the features of the BeBionic such as current limits and the ability to read values related to it make the hand suitable for human-environment interaction with a stiff grip. Even if this is the case the BeBionic hand design makes it complex to integrate them with a robotic system such as EVE. Parts such as the spring loaded fingers bypass any type of control in the finger extension motion under the presence of an external object flexing the finger. In addition, and bearing in mind the goal of introducing EVE in the healthcare environment, the BeBionic hands show limited features to establish reliable interactions with the environment, as some situations may require for a softer, more compliant grip than what the BeBionic is capable of rendering.

Interaction control such as impedance control cannot be implemented with the BeBionic hands due to its non-backdrivable nature. However, in section 1 another interaction control strategy, the *hybrid position/force control*. Such a control strategy could be implemented making use of the unitless currents provided by the BeBionic and the kinematic model developed in this work. Future work should focus on the implementation of an interaction control pipeline for EVE to safely interact with the environment.

Moreover, this work has only shown the potential of the hands to identify the presence objects during grasping tasks and their material properties. The evaluation of this capability for the BeBionic hands was purely qualitative. A scientific evaluation of this potential should be carried in the future, where a clear classification of contact/non contact is provided based on the signals obtained from the hands. In order to do so a proper analysis on the dynamics of the interaction between the hands and different objects must be conducted. If this is implemented successfully the hands will be able to provide additional information about the physical properties of the objects being manipulated, enhancing the tactile capabilities of the robot.

Bibliography

[1] Ottobock. (2022) Bebionic hand eqd: The most lifelike prosthetic hand. [Online]. Available: https://www.ottobock.com/en-us/product/8E70

[2] R. Bogue, "Humanoid robots from the past to the present," *Industrial Robot: the international journal of robotics research and application*, vol. 47, no. 4, pp. 465–472, 2020.

[3] A. Billard and D. Kragic, "Trends and challenges in robot manipulation," *Science*, vol. 364, no. 6446, p. eaat8414, 2019.

[4] C. C. Kemp, A. Edsinger, and E. Torres-Jara, "Challenges for robot manipulation in human environments [grand challenges of robotics]," *IEEE Robotics & Automation Magazine*, vol. 14, no. 1, pp. 20–29, 2007.

[5] E. N. Gama Melo, O. F. Aviles Sanchez, and D. Amaya Hurtado, "Anthropomorphic robotic hands: a review," *Ingeniería y desarrollo*, vol. 32, no. 2, pp. 279–313, 2014.

[6] T. Yoshikawa, "Multifingered robot hands: Control for grasping and manipulation," *Annual Reviews in Control*, vol. 34, no. 2, pp. 199–208, 2010.

[7] H. Robotics. (2022) Eve: Safe, capable and affordable humanoid robot platform. [Online]. Available: https://www.halodi.com/eve

[8] K. J. Waldron and J. Schmiedeler, "Kinematics," in *Springer handbook of robotics*. Springer, 2016, pp. 11–36.

[9] C. Rocha, C. Tonetto, and A. Dias, "A comparison between the denavit–hartenberg and the screw-based methods used in kinematic modeling of robot manipulators," *Robotics and Computer-Integrated Manufacturing*, vol. 27, no. 4, pp. 723–728, 2011.

[10] N. B. Figueroa, F. Schmidt, H. Ali, and N. Mavridis, "Joint origin identification of articulated robots with marker-based multi-camera optical tracking systems," *Robotics and Autonomous Systems*, vol. 61, no. 6, pp. 580–592, 2013.

[11] X. Zhang, S.-W. Lee, and P. Braido, "Determining finger segmental centers of rotation in flexion–extension based on surface marker measurement," *Journal of biomechanics*, vol. 36, no. 8, pp. 1097–1102, 2003.

[12] J.-S. Won and S. Lee, "Geometry-based finger kinematic models for joint rotation configuration and parameter estimation," *International Journal of Advanced Robotic Systems*, vol. 17, no. 4, p. 1729881420930576, 2020.

[13] A. Ude, C. Man, M. Riley, and C. G. Atkeson, "Automatic generation of kinematic models for the conversion of human motion capture data into humanoid robot motion," Georgia Institute of Technology, Tech. Rep., 2000.

[14] J. F. O'Brien, R. E. Bodenheimer Jr, G. J. Brostow, and J. K. Hodgins, "Automatic joint parameter estimation from magnetic motion capture data," Georgia Institute of Technology, Tech. Rep., 1999.

[15] M. Tuceryan, D. S. Greer, R. T. Whitaker, D. E. Breen, C. Crampton, E. Rose, and K. H. Ahlers, "Calibration requirements and procedures for a monitor-based augmented reality system," *IEEE Transactions on Visualization and Computer Graphics*, vol. 1, no. 3, pp. 255–273, 1995.

[16] L. Y. Chang and N. S. Pollard, "Constrained least-squares optimization for robust estimation of center of rotation," *Journal of biomechanics*, vol. 40, no. 6, pp. 1392–1400, 2007.

[17] S. S. H. U. Gamage and J. Lasenby, "New least squares solutions for estimating the average centre of rotation and the axis of rotation," *Journal of biomechanics*, vol. 35, no. 1, pp. 87–93, 2002.

[18] L. Y. Chang and N. S. Pollard, "Robust estimation of dominant axis of rotation," *Journal of biomechanics*, vol. 40, no. 12, pp. 2707–2715, 2007.

[19] B. Armstrong-Hélouvry, P. Dupont, and C. C. De Wit, "A survey of models, analysis tools and compensation methods for the control of machines with friction," *Automatica*, vol. 30, no. 7, pp. 1083–1138, 1994.

[20] G. Antonelli, F. Caccavale, and P. Chiacchio, "A systematic procedure for the identification of dynamic parameters of robot manipulators," *Robotica*, vol. 17, no. 4, pp. 427–435, 1999.

[21] H. Kawasaki and K. Nishimura, "Terminal-link parameter estimation of robotic manipulators," *IEEE Journal on Robotics and Automation*, vol. 4, no. 5, pp. 485–490, 1988.

[22] S. Chan, "An efficient algorithm for identification of robot parameters including drive characteristics," *Journal of Intelligent and Robotic Systems*, vol. 32, no. 3, pp. 291–305, 2001.

[23] M. Grotjahn, M. Daemi, and B. Heimann, "Friction and rigid body identification of robot dynamics," *International journal of solids and structures*, vol. 38, no. 10-13, pp. 1889–1902, 2001.

[24] K. S. Arun, T. S. Huang, and S. D. Blostein, "Least-squares fitting of two 3-d point sets," *IEEE Transactions on pattern analysis and machine intelligence*, no. 5, pp. 698–700, 1987.

[25] F. Bernardini, J. Mittleman, H. Rushmeier, C. Silva, and G. Taubin, "The ball-pivoting algorithm for surface reconstruction," *IEEE transactions on visualization and computer graphics*, vol. 5, no. 4, pp. 349–359, 1999.

[26] B. O. Community, *Blender - a 3D modelling and rendering package*, Blender Foundation, Stichting Blender Foundation, Amsterdam, 2018. [Online]. Available: http://www.blender.org

[27] M. Controzzi, C. Cipriani, and M. C. Carrozza, "Miniaturized non-back-drivable mechanism for robotic applications," *Mechanism and Machine Theory*, vol. 45, no. 10, pp. 1395–1406, 2010.

[28] L. Márton and B. Lantos, “Control of mechanical systems with stribeck friction and backlash,” *Systems & Control Letters*, vol. 58, no. 2, pp. 141–147, 2009.

[29] V. Pratt, “Direct least-squares fitting of algebraic surfaces,” *ACM SIGGRAPH computer graphics*, vol. 21, no. 4, pp. 145–152, 1987.

Appendix A

Estimation of the axis of rotation

The derivation shown in the following section can be found in [17]. Given a set of point cloud represented by a set of P points attached to a rigid body over N frames, each point in time is represented by $v_k^p, \{p \in P, k \in N\}$. Assuming that the rigid body rotates around a single point, each point p has a candidate to this point, m^p. The rotation around this point m^p will ideally occur around the same axis n for every point. With this setup, it is possible to define a cost function described by the projection of the $v_p^k - m^p$ vector on the ideal vector **n**. In the ideal case these two are perpendicular, rendering a null dot product. This is reflected in the following cost function:

$$C = \sum_{p=1}^{P} \sum_{k=1}^{N} [(v_k^p - m^p)n]^2$$

Differentiating with respect to **n** to find the $\arg\min_n\{C\}$ provides:

$$\frac{\partial C}{\partial n} = 0$$

$$\sum_{p=1}^{P} \sum_{k=1}^{N} [(v_k^p - m^p)n](v_k^p - m^p) = 0$$

Differentiating with respect to m^p provides the equation:

$$\frac{\partial C}{\partial m^p} = 0$$

$$\sum_{p=1}^{P} \sum_{k=1}^{N} 2[v_k^p - m^p)n](-n) = 0$$

$$\sum_{k=1}^{N} -v_k^p n + \sum_{k=1}^{N} m^p n = 0$$

$$m^p n = \left(\frac{1}{N} \sum_{k=1}^{N} v_k^p \right) n = \overline{v^p} n$$

These two equations can be combined to find a cost function that fully depends on the vector **n** and the set of vectors v_k^p. In this form, the equation does not contain any unknown term besides **n** and a numerical optimization/regression can be computed to obtain this parameter.

$$\sum_{p=1}^{P}\sum_{k=1}^{N}(v_k^p n - \overline{v^p} n)v_k^p = 0$$

Using algebraic manipulations described in **citation**, this problem turns into a simple linear algebra problem of the form $An = 0$, where A gets the form shown in the equation below. One way to solve this problem is to perform SVD on the matrix A, the axis of rotation will correspond to the singular vector with the smallest singular value.

$$A = \sum_{p=1}^{P}\left[\left\{\frac{1}{N}\sum_{k=1}^{N} v_k^p (v_k^p)^T\right\} - \overline{v^p}(\overline{v^p})^T\right]$$

Appendix B

Estimation of the centre of rotation

The derivation shown in the following section can be found in [16] The authors implement a non-rigid sphere fitting to a set of P markers over N time frames. They follow the work in [17] by combining Gamage et al. cost function with their own. Rather than using parameters **m** and **r** to parameterize the error, they use the sphere fitting approach described in [29].

Given the general description of a sphere as:

$$(x - x_c)^2 + (y - y_c)^2 + (z - z_c)^2 - r^2 = 0$$

It can be rewritten dependant to a set of parameters gathered in $\mathbf{u} = (a, b, c, d, e)^T$ to redefine the circle formula as:

$$aw + bx + cy + dz + e = 0$$

where the value $w = x^2 + y^2 + z^2$. One can define the algebraic distance $\delta(u)$ as how well the parameters in **u** are fit to a data point **v**. An estimate of the sphere fit which minimizes the sum of squared algebraic distances over every time frames. The parameter a is free to choose as a constraining constant (read paper to check exactly why). This is translated in the following equation:

$$b^2 + c^2 + d^2 + 4ea = 1$$

The least squares problem can be implemented as follows provided N frames. First the set of algebraic distances corresponding to the N frames of a single marker can be described in matrix form as:

$$\begin{bmatrix} \delta_1 \\ \vdots \\ \delta_k \\ \vdots \\ \delta_N \end{bmatrix} = \begin{bmatrix} w_1 & x_1 & y_1 & z_1 & 1 \\ \vdots & \vdots & \vdots & \vdots & \vdots \\ w_k & x_1 & y_k & z_k & 1 \\ \vdots & \vdots & \vdots & \vdots & \vdots \\ w_N & x_N & y_N & z_N & 1 \end{bmatrix} u = Du$$

In order to minimise the squared algebraic distances to estimate the spherical fit to **u**:

$$(Du)^T(Du) = u^T D^T Du = u^T Su$$

The constraint equation can be represented by the following notation:

$$u^T Cu = \begin{bmatrix} a & b & c & d & e \end{bmatrix} \begin{bmatrix} 0 & & & & -2 \\ & 1 & & & \\ & \dots & 1 & \dots & \\ & & & 1 & \\ -2 & & & & 0 \end{bmatrix} \begin{bmatrix} a \\ b \\ c \\ d \\ e \end{bmatrix} = 1$$

For P markers the vector u is amplified as $u = (a, b, c, d, e_1, e_2, ..., e_p)^T$ and matrices too subsequently.

Appendix C

Multi-Marker Capture support design

The designed motion capture protocol required for the development of a support structure in order to be able to attach more than one marker to the same segment. The main requirement was that the markers were not placed in a co-linear distribution, but rather in a sparse non symmetric disposition for the minimisation algorithm used to be effective. The final designed is shown in figure C.1. A "T" shaped structure was designed with flat surfaces were the markers were attached useing double sided tape.

Two pairs of support structures were designed, one for the thumb and the other for the rest of the fingers, as the dimensions of some of them matched. The dimensions of the supports allow for a sparse enough disposition of the markers so that there is no overlap between their signals on the motion capture system, but small and light enough to prevent the motion of the fingers to be affected in any manner. Specially the weight of the support plus markers was of importance, as in the finger flexion direction for the four non-opposable fingers are spring loaded. These fingers are susceptible to deform the spring under the presence of any extra weight in certain configurations of the hand in space, introducing bias in the measurements for the kinematic mapping.

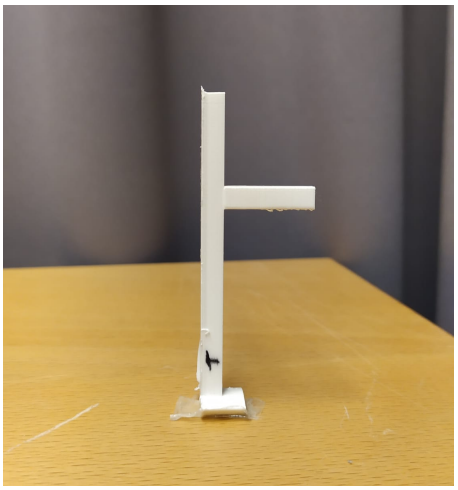

Figure C.1: Support structure for the placement of 3 markers on each hand segment